SUPPLEMENTARY INFORMATION TO:

β-catenin-driven differentiation is a tissue-specific epigenetic vulnerability in adrenal cancer

Dipika R. Mohan[1,2], Kleiton S. Borges[3,4], Isabella Finco[5], Christopher R. LaPensee[5], Juilee Rege[6], April L. Solon[7], Donald W. Little III[5], Tobias Else[5], Madson Q. Almeida[8,9], Derek Dang[10,11], James Haggerty-Skeans[1,10,11], April A. Apfelbaum[2,12], Michelle Vinco[10], Alda Wakamatsu[13], Beatriz M. P. Mariani[8], Larissa Costa Amorim[8,9], Ana Claudia Latronico[8], Berenice B. Mendonca[8], Maria Claudia N. Zerbini[13], Elizabeth R. Lawlor[12,14], Ryoma Ohi[7], Richard J. Auchus[5,15,16], William E. Rainey[6], Suely K. N. Marie[17], Thomas J. Giordano[5,10,18], Sriram Venneti[6,10,11,19], Maria Candida Barisson Villares Fragoso[8,9], David T. Breault[3,4,20], Antonio Marcondes Lerario[5,21]*, and Gary D. Hammer[5,6,7,18,21]*

University of Michigan, Ann Arbor, MI, USA: [1]Medical Scientist Training Program; [2]Doctoral Program in Cancer Biology; [5]Department of Internal Medicine, Division of Metabolism, Endocrinology, and Diabetes; [6]Department of Molecular and Integrative Physiology; [7]Department of Cell & Developmental Biology; [10]Department of Pathology; [11]Laboratory of Brain Tumor Metabolism and Epigenetics; [16]Department of Pharmacology; [18]Rogel Cancer Center Endocrine Oncology Program; [19]Department of Pediatrics and Communicable Diseases

Ann Arbor, MI, USA: [15]Lieutenant Colonel Charles S. Kettles Veterans Affairs Medical Center

Harvard Medical School, Boston, MA, USA: [3]Division of Endocrinology, Boston Children's Hospital; [4]Department of Pediatrics; [20]Harvard Stem Cell Institute

University of Washington, Seattle, WA, USA: [12]Seattle Children's Research Institute; [14]Department of Pediatrics

Faculdade de Medicina da Universidade de São Paulo, SP, Brazil: [8]Unidade de Suprarrenal, Laboratório de Hormônios e Genética Molecular/LIM42, Hospital das Clínicas, Departamento de Clínica Médica, Disciplina de Endocrinologia; [9]Instituto do Câncer do Estado de São Paulo (ICESP); [13]Departamento de Patologia; [17]Laboratório de Biologia Molecular e Celular/LIM15, Departamento de Neurologia

[21]Co-senior authors

*Correspondence:

Antonio Marcondes Lerario, MD, PhD, 1860 Taubman Biomedical Science Research Bldg, 109 Zina Pitcher Pl, Ann Arbor, MI 48109-2200, USA. Phone: +1 (734) 763-6289. Email: alerario@umich.edu

Gary D. Hammer, MD, PhD, 1528 Taubman Biomedical Science Research Bldg, 109 Zina Pitcher Pl, Ann Arbor, MI 48109-2200, USA. Phone: +1 (734) 615-2421. Email: ghammer@umich.edu

Supplemental information includes:

- Supplementary Figures 1-6 with Figure Legends
- Supplementary Table 1 (reference only), Supplementary Table 2
- Supplementary Methods
- Supplementary References

SUPPLEMENTARY FIGURES AND LEGENDS

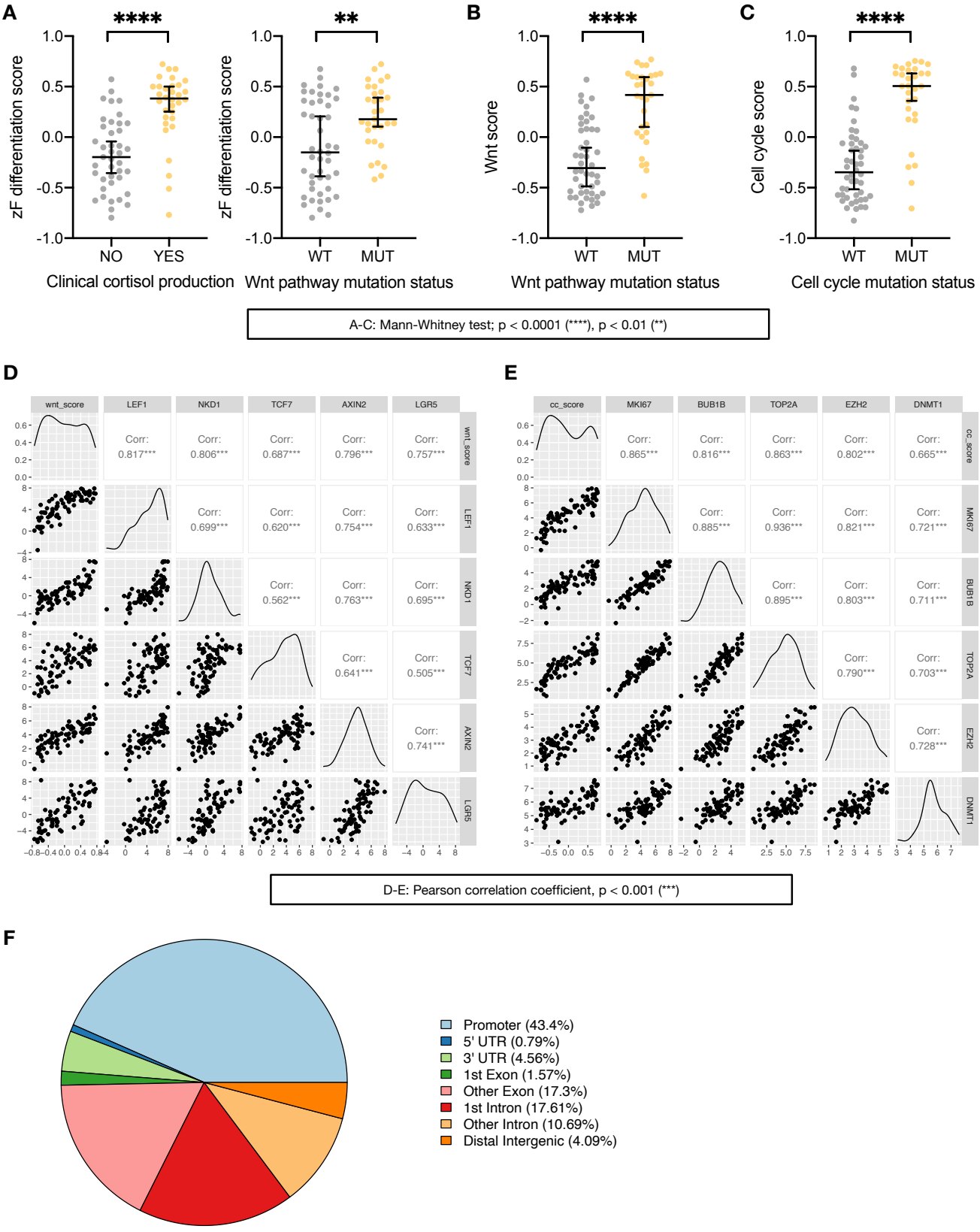

Supplementary Figure 1: Validation of ACC-TCGA scores, related to Figure 1

A-C. Genes comprising zF differentiation score, Wnt score, and cell cycle score were identified and calculated as described in Methods. Shown in A, zF differentiation score is significantly higher in ACC-TCGA tumors with clinical cortisol production, left, and Wnt pathway alterations (WT=Wnt wild type, MUT=driver alterations in *CTNNB1*, *APC*, or *ZNRF3*), right. Shown in B, Wnt score is significantly higher in ACC-TCGA

tumors with Wnt pathway alterations. Shown in C, cell cycle score is significantly higher in ACC-TCGA tumors with cell cycle alterations (WT=Cell cycle wild type, MUT=driver alterations in *TP53*, *RB1*, *CDKN2A*, *CCNE1*, *CDK4*).

D. Across ACC-TCGA, Wnt score exhibits strong correlation with expression of *bona fide* canonical Wnt target genes.

E. Across ACC-TCGA, Cell cycle score exhibits strong correlation with expression of *bona fide* cell cycle markers (*MKI67*, *BUB1B*, *TOP2A*) and epigenetic modifiers (*EZH2*, *DNMT1*).

F. Characteristics of PRC2 target CpGi probes depicted in **Figure 1D**. As expected, probes are predominantly located in promoter regions (>40%).

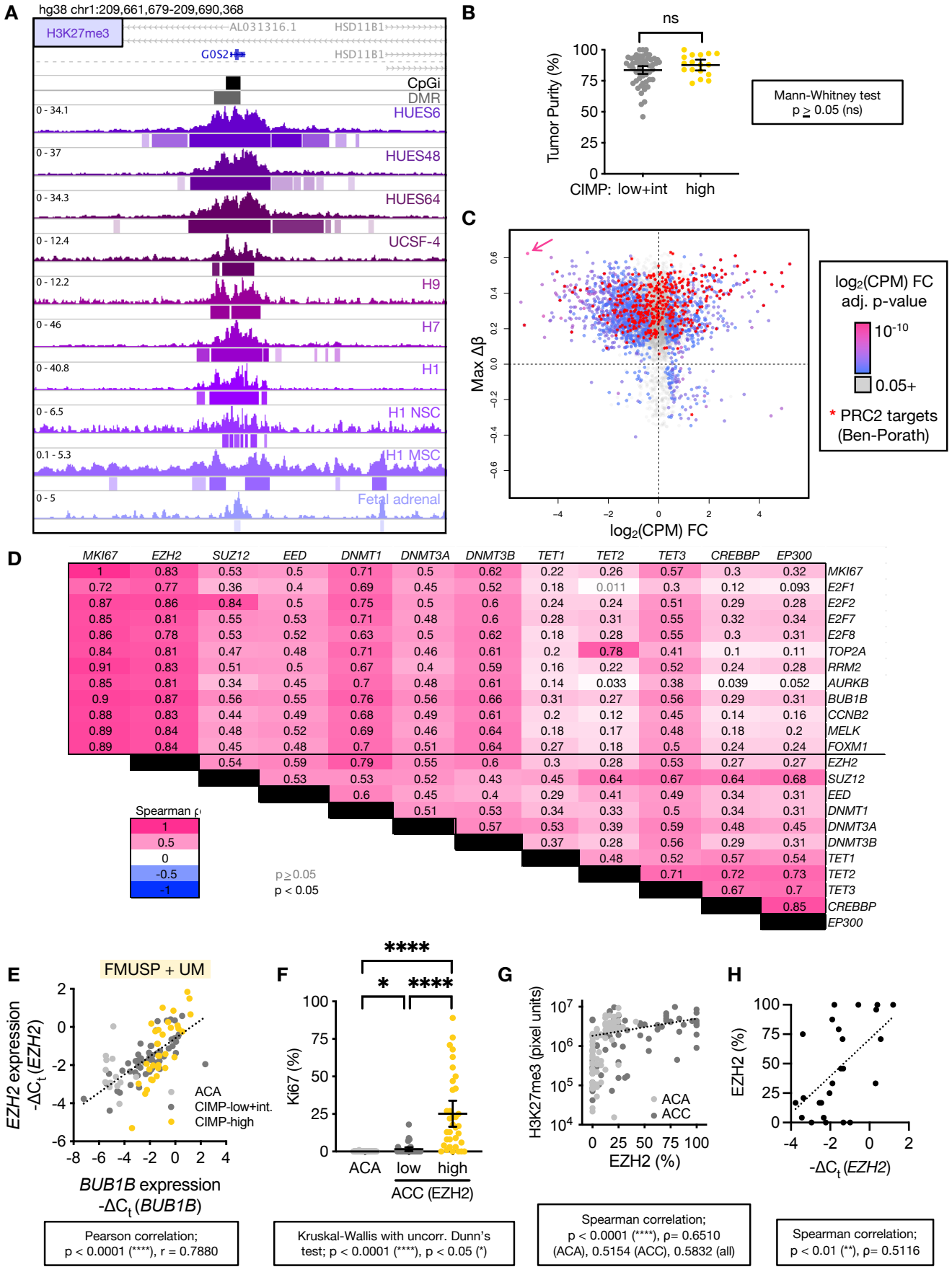

Supplementary Figure 2: Related to Figure 1

A. Example H3K27me3 ChIP-seq signal at the *G0S2* locus in human embryonic stem cells (ESC, includes HUES6, HUES48, UCSF-4, H9, H7, H1), ESC-derived neuronal stem cells (H1 NSC), ESC-derived

mesenchymal stem cells (H1 MSC), and the fetal adrenal. Location of *G0S2* CpG island in black (top track), with region targeted for methylation in CIMP-high ACC depicted in grey (DMR, second track). Peak calls are depicted by bars below each track. Hg38-aligned ChIP-seq data and peak calls downloaded from ENCODE (1,2).

B. Tumor purity across non-CIMP-high and CIMP-high ACC from ACC-TCGA (3). Line at mean with 95% confidence interval (CI).

C. Scatterplot depicts max change in DNA methylation (max Δβ) between CIMP-high and non-CIMP-high ACC at promoter DMRcate regions (queried by GSEA in **Figure 1C** and originally reported in (4)) versus $\log_2$ of the fold change in gene expression (measured by counts per million, CPM) between CIMP-high and non-CIMP-high ACC, color-coded by the p-value for the fold change in gene expression. PRC2 targets (from BENPORATH_PRC2_TARGETS set (5) deposited in MSigDB) are indicated by red stars. *G0S2*, silenced by methylation in CIMP-high ACC, is indicated by the arrow.

D. Pan-cancer correlation matrix depicting relationship between cell cycle genes (*MKI67, E2F1, E2F2, E2F7, E2F8, TOP2A, RRM2, AURKB, BUB1B, CCNB2, MELK, FOXM1*) and genes encoding epigenetic modifiers (*EZH2, SUZ12, EED, DNMT1, DNMT3A, DNMT3B, TET1, TET2, TET3, CREBBP, EP300*) across TCGA. Expression data with Spearman ρ and p-value for each pairwise comparison were mined and computed with GEPIA (6).

E. *EZH2* expression vs. expression of cell cycle-dependent gene *BUB1B* across adrenocortical tumors measured by qPCR in our independent cohort. Cohort with *BUB1B* expression data originally published in (4).

F. Ki67 proliferation index (% nuclei Ki67+) across ACA and primary ACC stratified by EZH2 expression in TMA. EZH2 low=ACC with below median EZH2 expression ($\leq$ 25% nuclei EZH2+), EZH2 high=ACC with above median EZH2 expression (> 25% nuclei EZH2+). ACA, n=74; EZH2 low ACC, n=37; EZH2 high ACC, n=35.

G. Scatterplot depicting correlation between H3K27me3 signal and EZH2 protein expression in samples in TMA. Data quantified as detailed in **Figure 1F-G**.

H. Scatterplot depicting correlation between EZH2 protein and *EZH2* mRNA expression levels from patients for which there was protein data from formalin-fixed, paraffin-embedded samples in the TMA (**Figure 1F-G**) and mRNA data harvested from frozen samples in the FMUSP+UM Cohort (**Figure 1E**).

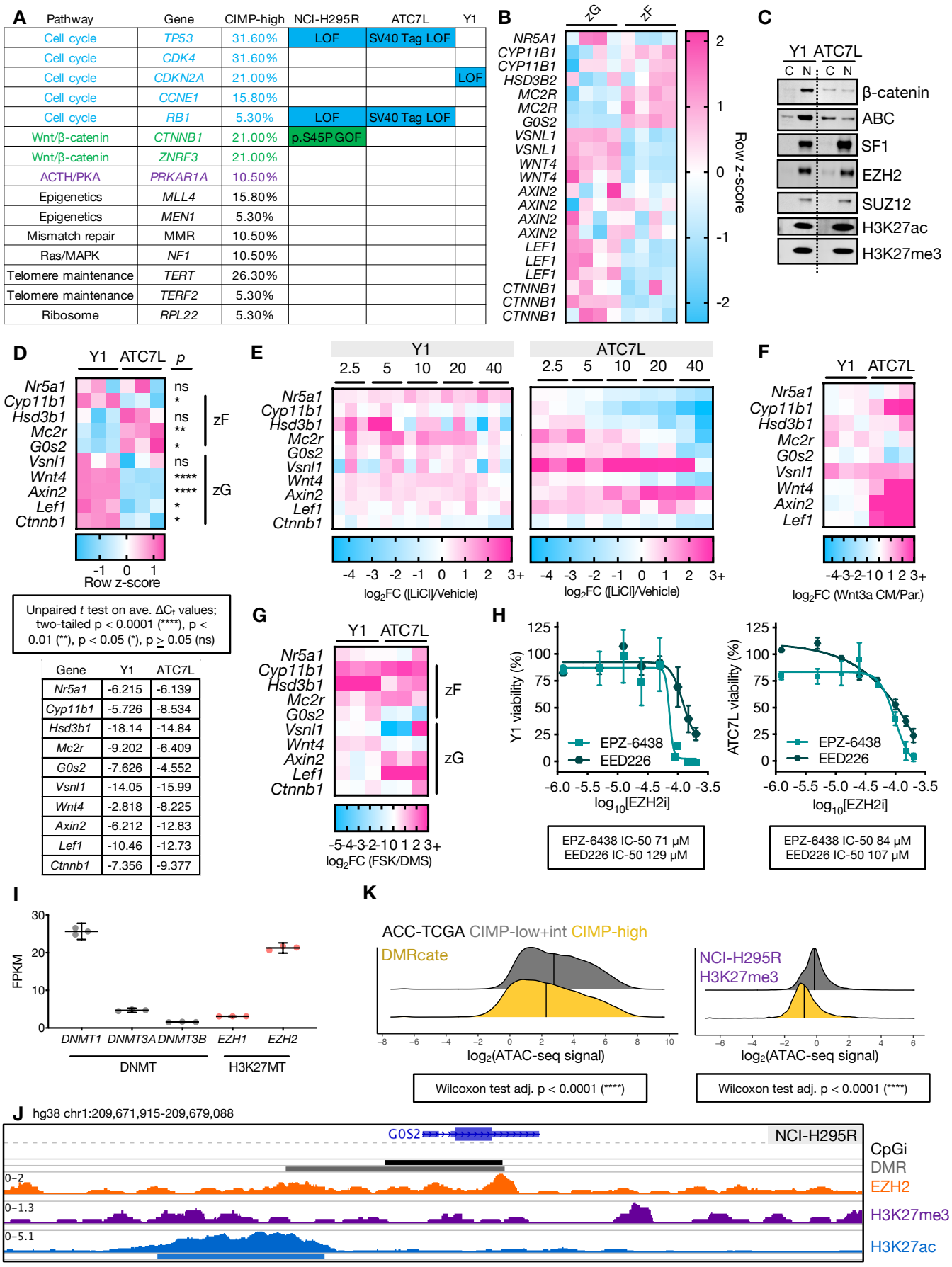

Supplementary Figure 3: Related to Figure 2

A. ACC cell lines resemble CIMP-high ACC. Table includes list of recurrently altered genes identified in ACC-TCGA (3). Third column describes the frequency of driver somatic alteration affecting that gene in CIMP-high ACC (3). Genetic alterations for NCI-H295R and Y1 cell lines were identified and confirmed by inspecting BAM files from RNA-seq data generated by our group and others (7). Next-generation sequencing data is not available for ATC7L cell line and genetic alterations are therefore predicted based on known biological features of this line. Importantly, ATC7L is unlikely to harbor alterations leading to autonomous Wnt/β-catenin pathway activation since this line is very responsive to Wnt pathway stimulation (8).

B. Heatmap of human adrenal microarray data from (9). Genes were selected based on the literature and their involvement in pathways of interest. Genes encoding steroidogenic enzymes – *CYP11B1, HSD3B2*. Wnt/β-catenin pathway – *WNT4, AXIN2*, *LEF1*, *CTNNB1*. *G0S2* is targeted for methylation-dependent silencing in CIMP-high ACC, *NR5A1* encodes SF1, *MC2R* encodes the ACTH receptor, and *VSNL1* is a highly zG-specific gene upregulated in aldosterone-producing adrenocortical adenomas (10,11). By this analysis, "zF genes"=*CYP11B1, HSD3B2, MC2R, G0S2* and "zG genes"=*VSNL1, WNT4, AXIN2, LEF1, CTNNB1*.

C. Y1 and ATC7L cells were fractionated into cytoplasmic (C) and nuclear (N) compartments, and protein lysates prepared from each compartment were analyzed by western blot, 15 µg protein loaded per lane. For each epitope, Y1 and ATC7L lysates were run on the same gel/membrane. Irrelevant lanes between the two sets of samples are cropped at the dashed line. Y1 express high levels of nuclear β-catenin, measured by total β-catenin in the top row, and active β-catenin (ABC) in second row; ATC7L express substantially lower levels of nuclear β-catenin. SF1 and PRC2 are nuclear and relatively comparable across both cell lines. H3K27ac and H3K27me3 are also comparable across cell lines and are shown here to demonstrate purity of cytoplasmic fraction.

D. ATC7L bears stronger zF differentiation than Y1. Top, heatmap of row z-score for qPCR data measuring expression of zonally expressed genes. Note that the genomic context of *Hsd3b1* (BLAST alignment with *HSD3B2* locus including upstream enhancer, data not shown) and its expression pattern render it the murine ortholog of *HSD3B2* (12). Bottom, average $-\Delta C_t$ values for gene expression z-score calculated in top. Gene expression was measured by qPCR on reverse transcribed total mRNA from 3 independent biological replicates of ATC7L and Y1 cell lines grown in culture under standard conditions.

E-F. ATC7L (and not Y1) respond to Wnt pathway activation with partial zG differentiation at the expense of zF differentiation. Y1 (E, left) or ATC7L (E, right) were stimulated overnight (18.5-19.5 hrs) with LiCl and harvested for total mRNA and evaluation of gene expression by qPCR. LiCl is a potent and well characterized inhibitor of GSK3β, a core member of the destruction complex that targets β-catenin for degradation in the absence of Wnt ligands; LiCl administration mimics Wnt pathway activation (13). Concentration of LiCl in mM is indicated above each set of biological replicates (n=3 for Y1, n=2 for ATC7L) and heatmap is color coded by $\log_2$ of the fold change between the given concentration of LiCl over vehicle according to the legend below each plot. In E, right, ATC7L exhibits a dose dependent increase in expression of zG genes and canonical Wnt targets like *Axin2*, at the expense of zF genes. In contrast, Y1 (E, left) changes in gene expression in response to LiCl are minimal and encompass a broad upregulation of both zG and zF genes. In F, ATC7L and Y1 were stimulated with 20% Wnt3a conditioned medium (Wnt3a CM) or negative control (parental medium without Wnt3a, Par.), for 24 hours and harvested for total mRNA and evaluation of gene expression by qPCR. n=3 biological replicates for each cell line, and heatmap is color coded by $\log_2$ of the fold change between Wnt3a CM and Par. according to the legend below each plot. As in E, Wnt pathway activation could induce expression of zG genes in ATC7L only and had minimal effect on Y1 cells.

G. Y1 (and not ATC7L) exhibits exclusive induction of zF genes in response to PKA activation. Y1 and ATC7L were stimulated for 24-26 hours with 10 µM forskolin (FSK) or equivalent volume of vehicle (DMS) and harvested for total mRNA and evaluation of gene expression by qPCR. Forskolin is a well characterized stimulant of the PKA pathway, inducing intracellular accumulation of cAMP (14). Heatmap is color coded by $\log_2$ of the fold change between FSK over DMS according to the legend below each plot, n=3 for each cell line. Treatment of adrenocortical cell lines with forskolin imitates the actions of ACTH (15). Forskolin

administration in Y1 cells exclusively induced expression of zF genes; in contrast, forskolin administration in ATC7L cells induced expression of zF and zG genes.

H. Viability curves for Y1 and ATC7L treated with different classes of EZH2 inhibitors (EZH2i). Data are represented by mean (point) with SEM (whiskers). N=3 for each inhibitor per cell line.

I. Gene expression (fragments per kilobase of transcript per million mapped reads, FPKM) values from baseline NCI-H295R RNA-seq (n=3 replicates) of DNA methyltransferases (DNMT) *DNMT1*, *DNMT3A*, *DNMT3B*, and histone methyltransferases (HMT) *EZH1* and *EZH2*.

J. Example EZH2, H3K27me3, and H3K27ac ChIP-seq tracks across the *G0S2* locus in baseline NCI-H295R. Location of *G0S2* CpG island in black (top track), with region targeted for methylation in CIMP-high ACC depicted in grey (DMR, second track). Peak calls are depicted by bars below each track.

K. Ridge plot of chromatin accessibility signal at DMRcate regions (left) or NCI-H295R peaks (right) in ACC-TCGA ATAC-seq samples (n=9, (16)). Line at median.

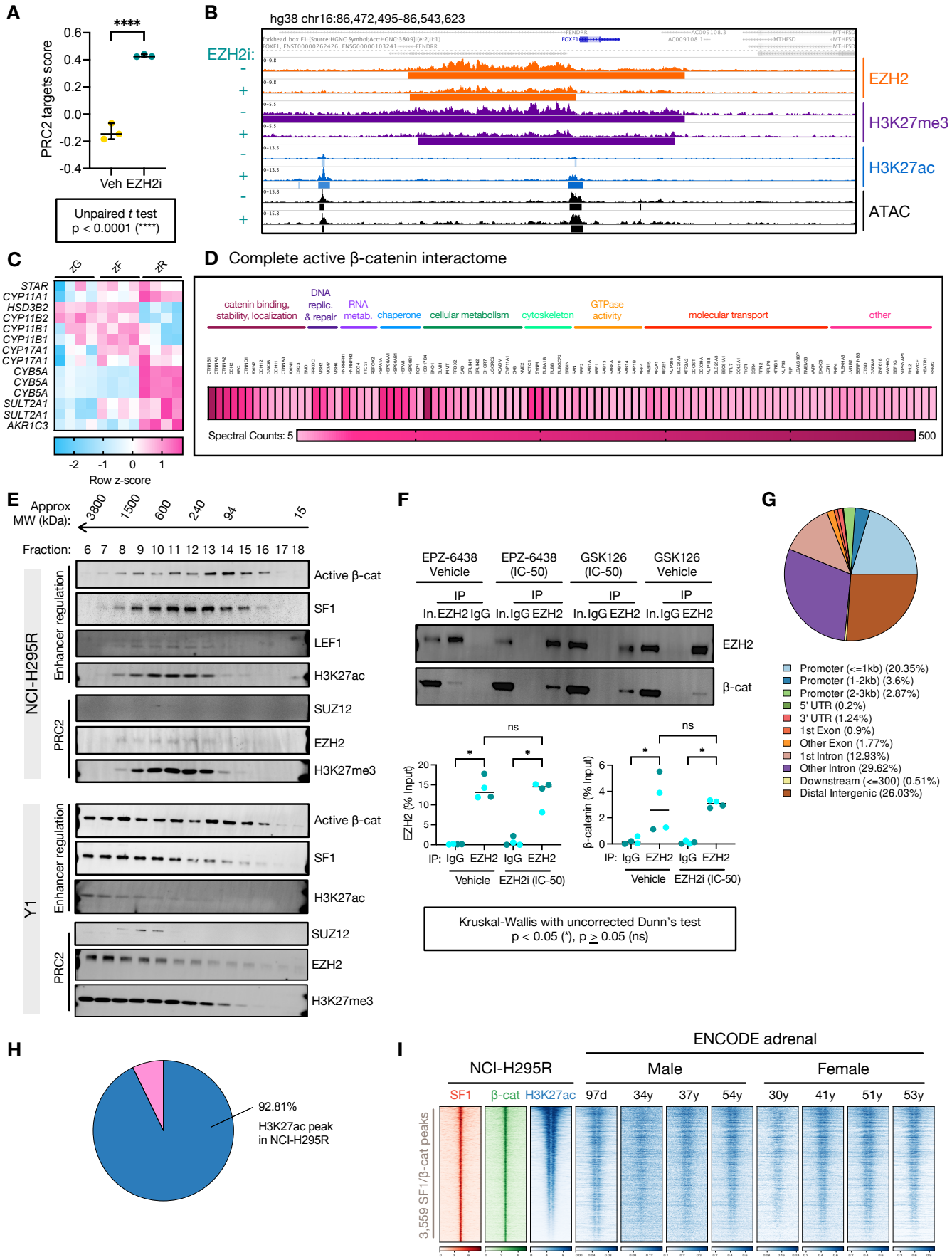

Supplementary Figure 4: Related to Figures 3-4

A. PRC2 targets score computed by GSVA (17) on RNA-seq data using BENPORATH_PRC2_TARGETS set (5) deposited in MSigDB in baseline (Veh=vehicle-treated) or EZH2i-treated NCI-H295R.

B. Example EZH2, H3K27me3, H3K27ac, and ATAC-seq tracks across PRC2 target *FOXF1* locus in NCI-H295R at baseline (vehicle-treated, EZH2i-) or following EZH2 inhibition (EZH2i+). Peak calls are depicted by bars below each track.

C. Analysis of microarray data from (9) demonstrates zonal expression of steroidogenic enzymes.

D. Peptides retrieved from active β-catenin-directed IP-MS on nuclear lysates from NCI-H295R.

E. Nuclear lysates from NCI-H295R or Y1 cell lines were fractionated by size exclusion chromatography. Equal volumes of each fraction in desired size range (15 kDa to 3800 kDa) were analyzed by western blot for epitopes shown right. Active β-cat=active β-catenin. As demonstrated in prior reports, PRC2 elution peaks at approximately 600 kDa (18). N=2.

F. Top, replicate western blot of EZH2 IP in vehicle- or EZH2i-treated (IC-50 dose) NCI-H295R as in **Figure 4D**. Lanes are 10% input (In), negative control IgG IP (IgG), EZH2 IP (EZH2) Bottom, quantification of western blot bands across all experimental replicates. Line at median. Color scheme as in **Figure 2D** (aqua points = GSK126, dark green points = EPZ-6438).

G. Characteristics of SF1/β-catenin binding sites in baseline NCI-H295R. 65% of peaks are >1000 bp away from a TSS and are therefore distal.

H. Pie chart depicting proportion of physiologic adrenal super-enhancers called by 3DIV analysis (19,20) on ENCODE samples (1,2) overlapping with H3K27ac peaks in baseline NCI-H295R.

I. Heatmap of SF1, β-catenin, and H3K27ac signal in baseline NCI-H295R or H3K27ac signal across human adrenal samples deposited in ENCODE (1,2) at 3,559 SF1/β-catenin cotargets, ranked by NCI-H295R H3K27ac signal. ENCODE samples from fetal male (97 day) and adult male and female (30-54 years of age). Centered at peak +/- 3 kb window.

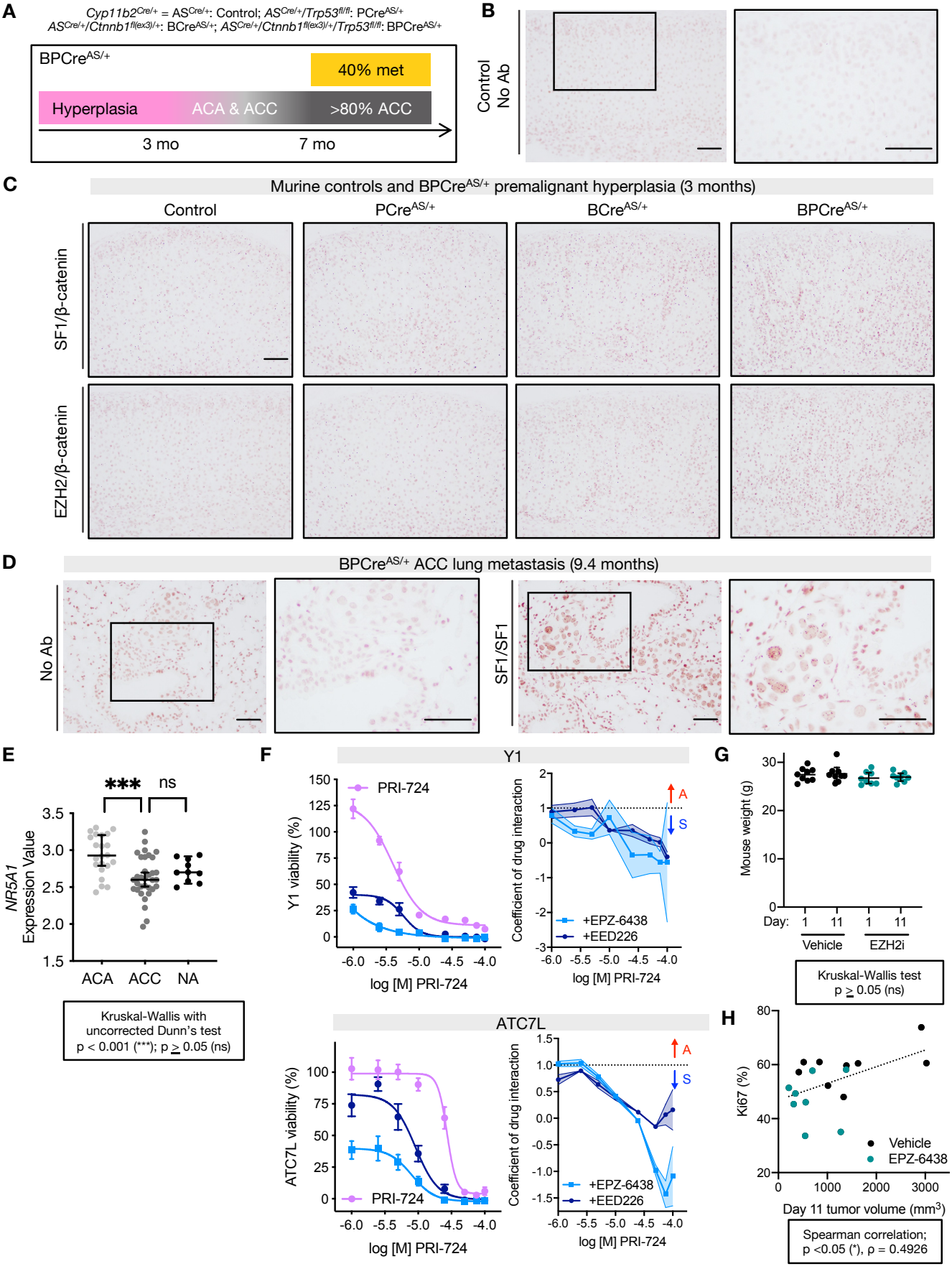

Supplementary Figure 5: Related to Figures 5-7

A. Top, key for abbreviations of mouse models used in the paper. Boxed, schematic of tumorigenesis in BPCre$^{AS/+}$ model (21). By age 3 months, all mice exhibit adrenocortical hyperplasia. At age 5-7 months,

approximately half of mice possess tumors (ACC and ACA). At 7-12 months, all mice possess tumors (with >80% meeting Weiss criteria for ACC) and 40% bear metastatic disease.

B. Example negative control PLA (no antibodies, No Ab) performed on sections from 3-month-old control ($AS^{Cre/+}$) mice adrenals. Negative control PLA performed on n>10 murine adrenal and adrenal tumor tissue samples. Bar=100 μm.

C. Low magnification representative images of SF1/β-catenin and EZH2/β-catenin PLA performed on 3-month-old adrenals. Control, n=4 mice; $PCre^{AS/+}$, n=3 mice; $BCre^{AS/+}$, n=3 mice; $BPCre^{AS/+}$, n=4 mice. Bar=100 μm.

D. Representative images of negative control (No Ab) and positive control (SF1/SF1) PLA performed on $BPCre^{AS/+}$ lung metastases, n=3 mice. Bar=100 μm.

E. Expression of *NR5A1* in adrenal tumors (ACA and ACC) and normal adrenal (NA) from (22).

F. Top left, viability curves for Y1 treated with increasing concentrations of CBP inhibitor (CBPi) PRI-724 +/- different classes of EZH2i (EPZ-6438 or EED226) at the IC-50 dose. Top right, coefficient of drug interaction (CDI) for change in viability. CDI>1 represents antagonism (A), CDI <1 represents synergy (S). Data are represented by mean (point) with SEM (whiskers or error bands). CBPi, n=6; CBPi + EPZ-6438, n=3; CBPi + EED226, n=3. Bottom left, viability curves for ATC7L treated with increasing concentrations of CBPi PRI-724 +/- different classes of EZH2i at the IC-50 dose. Bottom right, CDI for change in viability. Data are represented by mean (point) with SEM (whiskers or error bands). CBPi, n=3; CBPi + EPZ-6438, n=3; CBPi + EED226, n=3.

G. Mouse weight in BCH-ACC3A allograft experiment at beginning of experiment (Day 1) and end (Day 11) by treatment group.

H. Proliferation (measured by % nuclear Ki67 signal) vs final tumor volume across treatment groups in BCH-ACC3A allograft experiment.

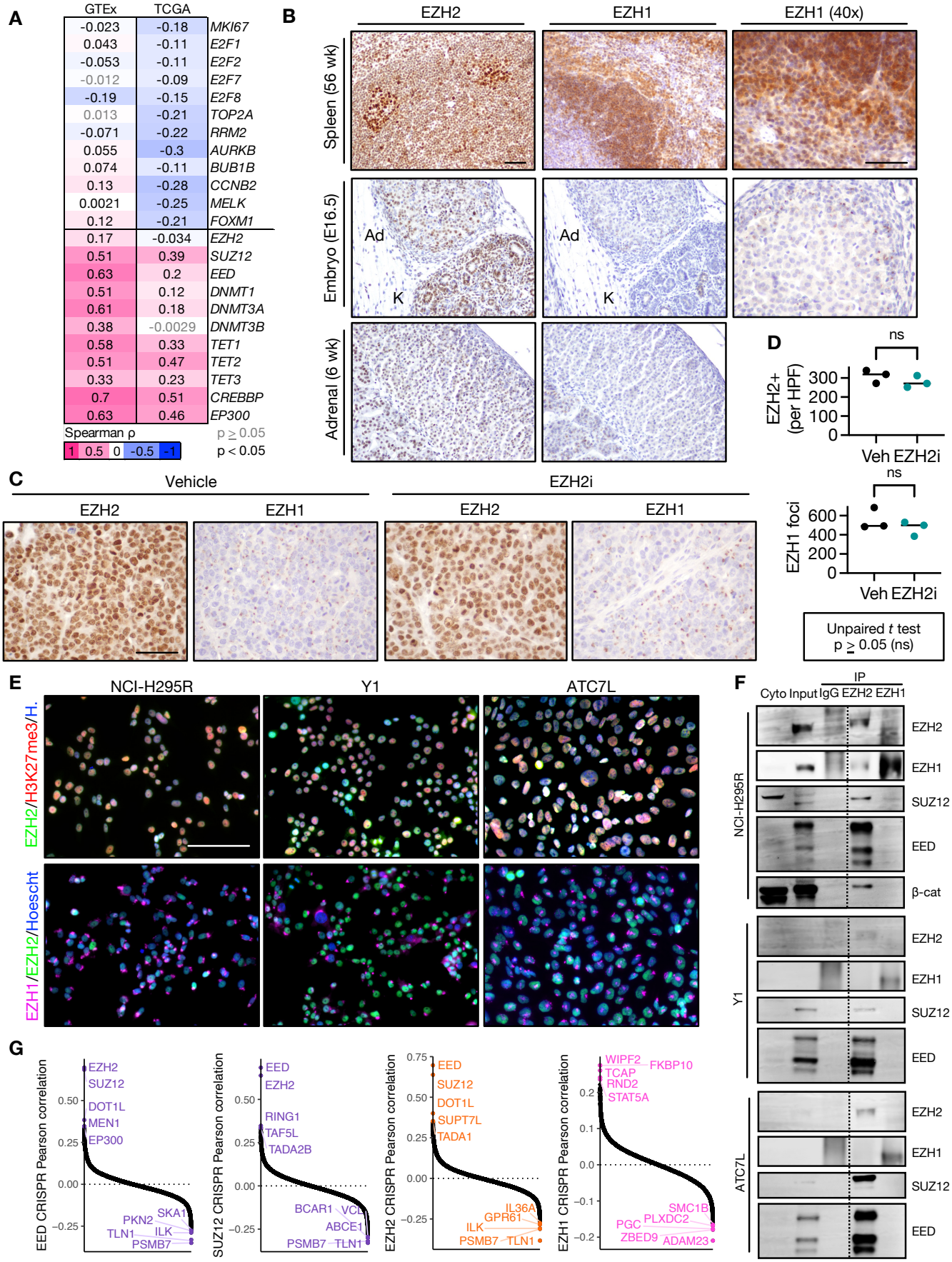

Supplementary Figure 6: Role of EZH1, related to Figures 1-7

A. Correlation matrix depicting relationship between *EZH1* and cell cycle genes (*MKI67, E2F1, E2F2, E2F7, E2F8, TOP2A, RRM2, AURKB, BUB1B, CCNB2, MELK, FOXM1*) and *EZH1* and genes encoding epigenetic

modifiers (*EZH2, SUZ12, EED, DNMT1, DNMT3A, DNMT3B, TET1, TET2, TET3, CREBBP, EP300*) across all normal tissues (GTEx) and cancer (TCGA). Expression data with Spearman ρ and p-value for each pair-wise comparison were mined and computed with GEPIA (6).

B. Representative images of EZH2 or EZH1 IHC in murine adult spleen (top), murine embryonic tissue (middle; Ad = adrenal, K = Kidney), and murine adult adrenal (bottom). Bar=100 μm.

C-D. In C, representative images and quantification of EZH2 or EZH1 IHC across treatment groups from **Figure 7**. Bar=100 μm. HPF = high-powered field. In D, each sample is represented by a point, line at median.

E. Representative immunocytochemistry in NCI-H295R, Y1 and ATC7L cell lines staining for nuclei (Hoescht, H), EZH2/H3K27me3 (top row) or EZH1/EZH2 (bottom row). Bar=100 μm.

F. Representative western blot of nuclear co-IP in NCI-H295R (top), Y1 (middle), and ATC7L (bottom) detecting EZH2, EZH1, SUZ12, EED and β-catenin (NCI-H295R only). Lanes are cytoplasmic fraction (collected as in **Supp Fig 3C** but not used for IP), 10% input, negative control co-IP (no antibody, IgG), EZH2 IP and EZH1 IP.

G. Correlation of CRISPR dependency scores from DepMap portal (23) across all genes and cancer cell lines for EED (left), SUZ12 (second from left), EZH2 (second from right) and EZH1 (far right). PRC2 components EZH2, EED, SUZ12 are all co-dependent with each other. In contrast, EZH1 is not co-dependent with any PRC2 components and vice versa.

SUPPLEMENTARY TABLES

Supplementary Table 1: NCI-H295R RNA-seq FPKM table, Related to Figures 2-4, 6.

See Excel sheet, uploaded separately.

Supplementary Table 2: qPCR Primers

Species	Gene	Orientation	Sequence (5'-3')
Mus musculus	*Nr5a1*	Forward	TGCAGAATGGCCGACCAG
Mus musculus	*Nr5a1*	Reverse	TACTGGACCTGGCGGTAGAT
Mus musculus	*Cyp11b1*	Forward	GCCATCCAGGCTAACTCAAT
Mus musculus	*Cyp11b1*	Reverse	CATTACCAAGGGGGTTGATG
Mus musculus	*Vsnl1*	Forward	CTGCAAAAAGCGACCCTTCC
Mus musculus	*Vsnl1*	Reverse	GTGTGCAGTCCATAGCATCG
Mus musculus	*Mc2r*	Forward	GTAAGTCAACGGCAAACACC
Mus musculus	*Mc2r*	Reverse	GTGTCATTGGTGTGTTCATACG
Mus musculus	*Lef1*	Forward	CTGAAATCCCCACCTTCTACC
Mus musculus	*Lef1*	Reverse	TGGGATAAACAGGCTGACCT
Mus musculus	*G0s2*	Forward	CACCCTAGGCCCAGCCA
Mus musculus	*G0s2*	Reverse	ACACTGCCCAGCACGTATAG
Mus musculus	*Actb*	Forward	CACTGTCGAGTCGCGTCC
Mus musculus	*Actb*	Reverse	TCATCCATGGCGAACTGGTG
Mus musculus	*Hsd3b1*	Forward	GAAGCTGCCCCTGATCTTTTC
Mus musculus	*Hsd3b1*	Reverse	GACAGTGGGAGCTGGTATGA T
Mus musculus	*Axin2*	Forward	GCAGGAGCCTCACCCTTC
Mus musculus	*Axin2*	Reverse	TGCCAGTTTCTTTGGCTCTT
Mus musculus	*Wnt4*	Forward	CTGGACTCCCTCCCTGTCTT
Mus musculus	*Wnt4*	Reverse	ATGCCCTTGTCACTGCAAA
Mus musculus	*Ctnnb1*	Forward	GCAGCAGCAGTTTGTGGA
Mus musculus	*Ctnnb1*	Reverse	TGTGGAGAGCTCCAGTACACC
Homo sapiens	*HSD3B2*	Forward	CTTTTAACAATCTAAGTTACGCCCT
Homo sapiens	*HSD3B2*	Reverse	AGTAGCAGGAAACACTTGCCA
Homo sapiens	*APCDD1*	Forward	CCAGAGGATGTTCTACCGGC
Homo sapiens	*APCDD1*	Reverse	AGGCATGGTCGTGGTTCTTG
Homo sapiens	*AXIN2*	Forward	GCTAGCTGAGGTGTCGAAGCCC
Homo sapiens	*AXIN2*	Reverse	GGCCGAATGATTCCTGTCCCTC
Homo sapiens	*VSNL1*	Forward	CAGGATGGGGAAGCAGAATAGC
Homo sapiens	*VSNL1*	Reverse	GGGCAAACTTGGAGGCG
Homo sapiens	*FOXF1*	Forward	TATCAAGCAGCAGCCCCTGTC
Homo sapiens	*FOXF1*	Reverse	AGACAAACTCCTTTCGGTCACA
Homo sapiens	*LGR5*	Forward	TCCGATCGCTGAATTTGGCT
Homo sapiens	*LGR5*	Reverse	ACGACAGGAGGTTGGACGAT
Homo sapiens	*PPIB*	Forward	GGCCCAAAGTCACCGTCAAG
Homo sapiens	*PPIB*	Reverse	AGCCAAATCCTTTCTCTCCTGTA

SUPPLEMENTARY METHODS

In vitro and molecular studies

Protein extraction and quantification. At endpoint, cells were washed with ice-cold PBS and incubated for 10 minutes on ice with ice cold whole-cell nuclear lysis buffer (50 mM Tris-HCl pH 8.1, 10 mM EDTA, 1% SDS in ultrapure H2O, adapted from (24)), supplemented with protease inhibitors (Roche cOmplete, Mini EDTA-Free, 04693159001) and phosphatase inhibitors (Roche PhosSTOP, 04906845001). Cells were scraped off plate in lysis buffer and transferred to microcentrifuge tubes. Samples were sonicated for 10 seconds at setting 70-80, placed on ice; this was repeated 2 additional times per sample. After sonication, lysates were stored on ice for 10 minutes, and then centrifuged at 14,000xg at 4°C for 15 minutes to remove insoluble debris. Supernatants were collected in fresh tubes. Alternatively, cells were washed with PBS containing phosphatase inhibitors (prepared using reagents provided in ActiveMotif, 54001), scraped into microcentrifuge tubes, pelleted by centrifugation at 1200xg for 5 minutes, frozen at -80°C, and later extracted for protein using complete whole-cell nuclear lysis buffer as stated above. Alternatively, cells washed with PBS, incubated on ice with complete whole-cell nuclear lysis buffer, scraped into microcentrifuge tubes, frozen at -80°C and protein extraction was later resumed as stated above. Alternatively, cytoplasmic and nuclear extracts were prepared using the ActiveMotif Nuclear Complex Co-IP Kit (ActiveMotif, 54001) according to manufacturer's protocol with specific details as follows: supernatant from spin after hypotonic lysis was saved as cytoplasmic fraction; enzymatic digests were performed at 4°C for 90 minutes. Prior to downstream processing, lysates and protein standards were quantified by BCA (Thermo, PI23227) in duplicate in 96 well plates. Briefly, 2 mg/mL standards were used to generate a 32 µg to 0 µg dilution series (in 50 µL); 2-5 µL of sample was diluted in 50 µL water. 200 µL of working reagent (prepared according to manufacturer instructions) were added to each well, plate was incubated at 37°C protected from light for 30 minutes, and absorbance was read at 562 nm using a VersaMax tunable microplate reader (Molecular Devices). Absorbance values of standard curve were used to determine sample concentration.

SDS-PAGE and western blot. Samples were prepared by boiling at 95°C for 6 minutes in lysis buffer supplemented with 4x Laemmli Sample Buffer (Bio-Rad, 161-0747, with 355 mM 2-mercaptoethanol freshly added) according to manufacturer's instructions. Alternatively, samples were boiled at 95°C for 5 minutes in 2X reducing buffer (130 mM Tris pH 6.8, 4% SDS, 0.02% bromophenol blue, with 0.1 M DTT freshly added) with 16.7% glycerol. Samples and a size marker (Bio-Rad, 1610374) were loaded onto NuPage 4-12% Bis-Tris gels (Invitrogen, NP0323 or NP0322) and run using the MOPS (Invitrogen, NP0001) or MES (Invitrogen, NP0002) buffer systems. Following SDS-PAGE, gels were Coomassie stained or transferred onto a PVDF membrane (Thermo, 88520) using a traditional wet transfer system and NuPage Transfer Buffer (Invitrogen, NP0006) supplemented with up to 20% methanol according to manufacturer instructions. Uniform transfer efficacy was verified by Coomassie staining of SDS-PAGE gel after transfer. Western blot was performed according to standard protocols, which typically consisted of 1 hour room temperature block, overnight

primary antibody incubation at 4°C, 4x5 minute washes, 1 hour secondary incubation at room temperature protected from light, 4x5 minute washes, 5 minute rinse, and visualization using the LI-COR Odyssey imaging system at 700 nm and/or 800 nm. Odyssey (TBS) Blocking Buffer (LI-COR, discontinued) or Intercept (TBS) Blocking Buffer (LI-COR, 927-60003) was used for blocking. Primary or secondary antibodies were diluted in blocking buffer + 0.1% Tween 20. TBS + 0.1% Tween 20 was used for wash steps, and TBS alone for the final rinse. The following antibodies were used for western blot: 1:1000 EZH2 (Cell Signaling Technology, 5246S, RRID:AB_10694683), 1:1000 EZH1 (Cell Signaling Technology, 42088, RRID:AB_2799212), 1:1000 SUZ12 (Cell Signaling Technology, 3737, RRID:AB_2196850), 1 µg/mL SUZ12 (R&D, MAB4184, RRID:AB_2196745), 1:8000 EED (PTG, 67756-1-Ig), 1:1000 active β-catenin (Cell Signaling Technology, 8814, RRID:AB_11127203), 1:1000 β-catenin (Invitrogen, MA1-2001, RRID:AB_326078), 1:500-1:2000 H3K27me3 (EMD Millipore, 07-449, RRID:AB_310624), 1:1000 H3K27ac (ActiveMotif, 39133, RRID:AB_2561016), 1:2000 SF1 (custom in-house antibody, RRID AB_2716716), 1-2 µg/mL SF1 (Thermo Fisher, 434200/N1665, RRID:AB_2532209), 1:1000 Lef1 (Cell Signaling Technology, 2230, RRID:AB_823558), 1:5000 β-actin (Sigma-Aldrich, A-5441, RRID:AB_476744), Western blot signal was quantified using the Analyze Gels tools in Fiji (RRID:SCR_002285) (25).

Coomassie staining. Coomassie staining was performed using Imperial Protein Stain (Thermo, 24615) according to manufacturer instructions. Briefly, SDS-PAGE gel was washed for 15 minutes with gentle shaking in ultrapure water. Gels were incubated with Imperial Protein Stain for 1-2 hours at room temperature with gentle shaking. Stain was discarded and replaced with ultrapure water and a folded Kimwipe Tissue. After overnight destaining, gels were imaged using the LI-COR Odyssey imaging system protein gel setting at 700 nm.

Size-exclusion chromatography. Nuclear lysates were clarified by centrifugation (16,000xg at 4°C for 5 minutes). Supernatant was subject to size exclusion chromatography on a Superose 6 column (GE Healthcare) equilibrated in a buffer of 20 mM HEPES (pH 7.9), 75 mM NaCl, and 1 mM DTT. Eluents spanning elution volumes 10 mL to 45 mL were collected and fractionated in 0.5 mL fractions. Approximate protein size of fractions was estimated using empirical calibration curve for the Superose 6 column, where M_r is estimated molecular weight in Daltons and V_e is 10 mL: $\log(M_r) = 0.40145*V_e-11.7996$. Fractions were analyzed by Coomassie staining and western blot.

Nuclear complex immunoprecipitation (co-IP). Nuclear co-IP was performed using the Nuclear Complex Co-IP Kit (ActiveMotif, 54001) and Protein G Agarose Columns (ActiveMotif, 53039) according to manufacturer's protocol with specific details as follows. Enzymatic digests were performed at 4°C for 90 minutes; co-IPs were performed using IP Low Buffer (ActiveMotif, 37511) for incubation and wash steps with no additional salts or detergents. 150-500 µg of nuclear lysate was used for IP, and antibody concentration was scaled

accordingly to maintain 3.5 µg antibody/275 µg nuclear lysate. Nuclear lysate concentration was quantified by BCA prior to setting up co-IP. Any of the following antibodies were used for Co-IP: EZH2 (Cell Signaling Technology, 5246S, RRID:AB_10694683), SUZ12 (Cell Signaling Technology, 3737, RRID:AB_2196850), SUZ12 (Bethyl, A302-407A, RRID:AB_1907290), active β-catenin (Cell Signaling Technology, 8814, RRID:AB_11127203), SF1 (custom in-house antibody, RRID:AB_2716716), EZH1 (Cell Signaling Technology, 42088, RRID:AB_2799212), negative control IgG (EMD Millipore, 12-370). Co-IPs were evaluated by mass spectrometry (IP-MS), or were eluted and evaluated by Coomassie staining and/or western blot.

Viability assays and calculations. Viability was measured using alamarBlue (Invitrogen, DAL1025) according to manufacturer's instructions. Briefly, at endpoint, media was changed to media containing alamarBlue at a concentration of 60 µL alamarBlue/600 µL media. Plate was incubated under standard culture conditions with protection from light for 2-4 hours (or until desired dye development was visible), and 100 µL of media was transferred in triplicate to a 96 well plate. Absorbance was measured using VersaMax tunable microplate reader (Molecular Devices) at 570 nm using 600 nm as a reference wavelength. % viability (%V) was calculated as follows. For vehicle or each treatment concentration, $AR=(\varepsilon_{OX,600})(A_{570}- B_{570}) - (\varepsilon_{OX,570})(A_{600}- B_{600})$, where $\varepsilon_{OX,600}$=117,216, $\varepsilon_{OX,570}$=80,586, A_{570}=absorbance of treatment well at 570 nm, B_{570}=absorbance of blank well (well containing no cells, only media and alamarBlue) at 570 nm, A_{600}=absorbance of treatment well at 600 nm, and B_{600}=absorbance of blank well at 600 nm. $\%V=100*AR_{treatment}/AR_{vehicle}$. Data were fitted to a 4PL sigmoidal curve using GraphPad and IC-50 was determined from interpolation of the curve to identify the concentration at 50% viability.

To evaluate drug interactions, a simplified coefficient of drug interaction (CDI) was calculated as described (26). Briefly, CDI between drugs C and D is given by the formula $CDI=\%V_{CD}/(\%V_C*\%V_D)$ where $\%V_{CD}$ is the %V when cells are treated with both drug C at dose x_1 and drug D at dose x_2, $\%V_C$ is the %V when cells are treated with drug C alone at dose x_1, and $\%V_D$ is the %V when cells are treated with drug D alone at dose x_2. CDI>1 signifies antagonism, CDI=1 signifies additivity, and CDI<1 signifies synergy. Negative CDI values are secondary to fluctuations of absorbance around the level of the blank when no viable cells remain in a well, and are consistent with CDI<1 for a drug that induces loss of viability. An alternative strategy would be to set the values of these conditions to 0.

Immunohistochemistry (IHC), RNA *in situ* hybridization, and proximity ligation assay

Brightfield IHC on TMAs. TMA of primary adrenocortical tumors from FMUSP was stained for EZH2 and H3K27me3 in triplicate. EZH2 staining was performed with 1:100 EZH2 (Cell Signaling Technology, 5246S, RRID:AB_10694683) using standard IHC deparaffinization/hydration protocols and the NovoLink Max Polymer Detection System (Leica Biosystems, Newcastle Ltd, RE7159) with the following modifications: All washes were performed with PBS. Antigen retrieval was performed using boiling Tris-EDTA, pH 9.0 (Spring

Bioscience, PMB4-235) for 35 minutes, endogenous peroxidase activity was quenched for 10 minutes at room temperature with 6% H_2O_2 in methanol. Blocking was performed for 10 minutes at 37°C with Cas Block (Invitrogen, 00-8120). Slides were incubated with primary antibody diluted in 1% BSA, 0.1% sodium azide in PBS for in a humidity chamber for 30 minutes at 37°C followed by 18 hours (overnight) at 4°C. Slides were then incubated in post-primary block (Leica, RE7159) and then Novolink Polymer (Leica, RE7161) for 30 minutes at 37°C each. A solution containing DAB (Sigma-Aldrich), 0.1% H_2O_2, and 0.06% DMSO in PBS served as the peroxidase substrate, developed for 5 minutes at 37°C. EZH2 expression levels were quantified on 0-4 scale based on % positive nuclei per section and averaged across two independent observers. H3K27me3 staining was performed as previously described (27). H3K27me3 levels were quantified by MATLAB as previously described (27).

Brightfield IHC on mouse tissues (excluding H3K27me3 on allografts). IHC was performed using the VECTASTAIN Elite ABC-HRP Kit, Peroxidase (Rabbit IgG) (Vector Labs, PK-6101) according to manufacturer's instructions with the following modifications: all kit reagents were prepared using PBS as the buffer, and washes were performed with PBS + 0.1% Tween-20. Antigen retrieval was performed with boiling 10 mM sodium citrate pH 6.0, 20 minutes, followed by benchtop cooling for 20 minutes. Endogenous peroxidase was quenched with 3% H_2O_2 in MilliQ water at room temperature for 20 minutes. Blocking was performed in a humidified chamber at room temperature for 2 hours. Primary antibody incubation (1:1000 SF1 custom in-house antibody, RRID:AB_2716716 or 1:200 Ki67 Thermo Fisher MA5-14520, RRID:AB_10979488) was performed in a humidified chamber at 4°C overnight, and secondary antibody incubation was performed in a humidified chamber at room temperature for 30 minutes. SIGMAFAST™ 3,3′-Diaminobenzidine (DAB) tablets (Sigma-Aldrich, D4168-50SET) served as the peroxidase substrate and were used according to manufacturer's instructions with same development time for all samples. Slides were equilibrated with tap water and counterstained with Gills #1 Hematoxylin for 10 seconds prior to dehydration. Slides were mounted with Vectamount Permanent Mounting Medium (Vector Labs, H-5000). Alternatively, IHC was performed as above using the ImmPRESS HRP Horse Anti-Rabbit IgG Polymer Detection Kit (Vector Labs, MP-7401), 10 mM sodium citrate pH 6.0 + 0.05% Tween-20 for antigen retrieval, and PBS for the wash steps. Blocking 1-2 hours. Primary antibody incubation (1:50 EZH2, Cell Signaling Technology, 5246, RRID:AB_10694683; 1:100 or 1:250 EZH1, Cell Signaling Technology, 42088, RRID:AB_2799212) was performed in a humidified chamber at 4°C overnight, and secondary antibody incubation was performed in a humidified chamber at room temperature for 30 minutes. ImmPACT DAB EqV (Vector Labs, SK-4103) served as the peroxidase substrate and was used according to manufacturer's instructions with the same development times per epitope per sample type. Slides were counterstained with hematoxylin for 30 seconds. DAB signal was quantified using a homemade macro in Fiji (25). Briefly, for Ki67 signal: Analysis performed on 10 40x images per mouse. Images were deconvoluted using H and DAB vectors, thresholded at (0, 225) and (0, 210) respectively, converted to mask, watershedded, and Analyze Particles function was used to count nuclei and

DAB staining (minimum particle size 400). DAB/nuclear signal was computed per image and averaged to yield a single value for each sample. Briefly, for SF1 signal: same as for Ki67 except images were thresholded at (0, 235) and (0, 180), respectively. Briefly, for EZH2 signal: same as for Ki67 except analysis was performed on 5 40x images per mouse, and only DAB signal was counted using a minimum particle size of 350 and threshold of (0, 145). Briefly, for EZH1 signal: same as for Ki67 signal except analysis performed on 5 20x images per mouse, images were deconvoluted using H and AEC vectors, AEC signal was thresholded automatically, and signal was counted using a minimum particle size of 25.

Brightfield H3K27me3 allograft IHC. Studies were performed as previously described (28,29). Briefly, immunohistochemistry was conducted using the Leica Bond automated staining processors (Leica Biosystems). Tissue sections were first blocked for 30min with 10% normal goat serum in 2% BSA in PBS. Sections were treated for 5h with anti-H3K27me3 (EMD Millipore, 07-449, RRID:AB_310624, 0.1µg/mL) and then for 60min with biotinylated goat anti-rabbit IgG (Vector Labs, PK6101) at 1:200 dilution. Blocker D, Streptavidin-HRP, and DAB detection kit (Ventana Medical Systems) kits were used as per manufacturers' instructions. Following this, slides were dried at room temperature and scanned. Images were captured and quantified in a blinded manner using automated scoring. Each section was scanned using an AperioScanscope Scanner (Aperio Vista) and visualized using the AperioImageScope software program. Three random JPEG images from each section at 40X magnification were captured by an individual blinded to the experimental setup and quantified with an automated analysis program with MATLAB's image processing toolbox (28,29). We used algorithms based on K-Means Clustering, color segmentation with RGB color differentiation, and background-foreground separation with Otsu's thresholding (28). The numbers of extracted pixels were then multiplied by their average intensity for each image and was represented as pixel units.

Immunofluorescence. Adrenals were fixed in 4% paraformaldehyde (PFA) for 2 hours (normal tissue, 24.3 week female in **Figure 5B**) or overnight (tumor, from 41.1 week male in **Figure 5B**), embedded in paraffin and cut into 5-µm sections. Antigen retrieval was performed in Tris-EDTA pH 9.0. Sections were blocked in 5% Normal Goat Serum, 0.1% Tween-20 in PBS for 1h at RT. For nuclear staining, DAPI (4′,6-diamidino-2-phenylindole) was added to secondary antibody mixture at a final concentration of 1:1000. Slides were mounted with ProLong Gold Antifade Mountant (Thermo Fisher Scientific, P36930). Primary antibodies: β-catenin (BD Biosciences, 610153, RRID:AB_397554), SF1 (Thermo Fisher, 434200/N1665, RRID:AB_2532209), H3K27me3 (Cell Signaling Technology, 9733, RRID:AB_2616029) and EZH2 (Cell Signaling Technology, 5246S, RRID:AB_10694683). Secondary antibodies: Alexa Fluor 647-conjugated goat anti-rabbit IgG (Invitrogen), Alexa Fluor 594-conjugated goat anti-mouse IgG (Invitrogen). Images were acquired using a Nikon upright Eclipse 90i microscope and entire images were adjusted for brightness and contrast in ImageJ (30).

Immunocytochemistry. Glass cover slips were sterilized, coated with poly-L-lysine (Sigma, P4707) per manufacturer instructions, and dried. Cells were plated onto glass cover slips. At endpoint, cover slips were rinsed with PBS and fixed with 10% neutral buffered formalin (room temperature with agitation for 10 minutes). Multiplex immunocytochemistry was performed using ImmPRESS HRP Horse Anti-Rabbit IgG Polymer Detection Kit (Vector Labs, MP-7401) and the ImmPRESS HRP Horse Anti-Mouse IgG Polymer Detection Kit (Vector Labs, MP-7402) according to manufacturer instructions with the following modifications: Cells were permeabilized with 0.2% Triton-X in PBS, and endogenous peroxidase activity was quenched with 3% H_2O_2 in MilliQ water at room temperature for 20 minutes. Blocking was performed in a humidified chamber at room temperature for 1 hour using 0.2% Triton-X, 10% Horse Serum in PBS. Primary antibody incubation (1:100 EZH2, Cell Signaling Technology, 5246S, RRID:AB_10694683; 1:100 EZH1, Cell Signaling Technology, 42088, RRID:AB_2799212; 1:750 H3K27me3, EMD Millipore, 07-449, RRID:AB_310624) was performed in a humidified chamber at 4°C overnight, and secondary antibody incubation was performed in a humidified chamber at room temperature for 30 minutes. Tyramide conjugated to Alexa Fluor 488 (Thermo Fisher, B40953) or 555 (Thermo Fisher, B40955) served as the HRP substrate. After TSA amplification, cover slips were washed and peroxidase was inactivated by incubation with 0.02 N HCl at room temperature for 20 minutes. Samples were again blocked, incubated with primary antibody, incubated with secondary antibody, and subject to TSA amplification using the alternate fluorophore. Nuclear counterstain was performed using Hoescht, and samples were mounted using 50% glycerol in PBS. Images were acquired using a Zeiss ApoTome microscope and images were adjusted for brightness and contrast in Fiji (25).

RNA in situ *hybridization in allografts*. RNA *in situ* hybridization was performed using the RNAscope 2.5 HD Assay – BROWN (Advanced Cell Diagnostics, 322310), associated reagents (Advanced Cell Diagnostics, 322335, 322335, 310091, 322001, 322331) according to manufacturer's instructions, and using probes for *Cyp11b1* (Advanced Cell Diagnostics, 564431), *Polr2a* (Advanced Cell Diagnostics, 312471), and *Dapb* (Advanced Cell Diagnostics, 310043). *Pol2ra* served as a positive control for intact RNA, and was abundantly detected in all samples; *Dapb* served as a negative control and was not detected in any samples. We observed that *Cyp11b1* is expressed in clusters of cells ("islands") in our allograft model, and quantified # of islands using a custom macro in Fiji (25). Briefly, samples were analyzed as for EZH1 signal, except 4 20x images were analyzed per mouse.

Proximity Ligation Assay (PLA). PLA was performed using the Duolink Detection Reagents Brightfield Kit (Sigma-Aldrich, DUO92012) and associated wash buffers (Sigma-Aldrich, DUO82047-4L) and PLA probes (Sigma-Aldrich, DUO92002, DUO92004) according to manufacturer protocol with the following modifications. Steps prior to blocking were performed per standard IHC protocol above, using PBS for wash steps prior to endogenous peroxide quench. Mouse samples: blocking was performed for 2 hours at room temperature

using a custom blocking buffer which was a 1:1 mixture of blocking buffers prepared from VECTASTAIN Elite ABC-HRP Kit, Peroxidase (Rabbit IgG) (Vector Labs, PK-6101) and the M.O.M. (Mouse on Mouse) Immunodetection Kit – Basic (Vector Laboratories, BMK-2022). Each blocking buffer is prepared at 2x the recommended concentration and combined 1:1 to create this custom blocking buffer. After blocking, samples were incubated with 1X M.O.M. diluent for 5 minutes at room temperature in a humidified chamber. Primary antibodies were diluted in M.O.M. diluent and incubated with slides overnight in a humidified chamber at 4°C. PLA probes were also diluted in M.O.M. diluent. Counterstain step was skipped because counterstain masked signal from nuclear epitopes. The following antibodies were used for PLA in dysplasia to carcinoma sequence: EZH2 (Cell Signaling Technology, 5246S, RRID:AB_10694683), β-catenin (BD Biosciences, 610154, RRID:AB_397554), SF1 (custom in-house antibody, RRID AB_2716716), SF1 (Thermo Fisher, 434200/N1665, RRID:AB_2532209). They were used at the following combinations: EZH2 (1:50)/β-catenin (1:50) to detect EZH2/β-catenin interactions, SF1 (1:500)/β-catenin (1:100) to detect SF1/β-catenin interactions, SF1 (Rb, 1:1500)/SF1 (Mmu, 1:100) to detect SF1+ cells in metastatic lesions, or no antibodies (No Ab) as a negative control.

Human samples: Performed as described for mouse samples with the following modifications. Blocking was performed using Duolink Blocking Buffer for 1 hour at 37°C per manufacturer instructions. PLA probes were diluted in Duolink Diluent per manufacturer instructions. The following antibodies were used for PLA in human tissue including FMUSP TMAs of primary and metastatic adrenocortical tumors in triplicate: EZH2 (Cell Signaling Technology, 5246S, RRID:AB_10694683), β-catenin (BD Biosciences, 610154, RRID:AB_397554), SF1 (custom in-house antibody, RRID AB_2716716). They were used at the following combinations: SF1 (1:1000)/β-catenin (1:100) to detect SF1/β-catenin interactions or EZH2 (1:100 - physiologic adrenal or 1:50 - TMA)/β-catenin (1:50) to detect EZH2/β-catenin interactions. Extensive optimization was performed on mouse and human tissue prior to arriving at optimal blocking conditions and antibody concentrations, including combining concentrations of antibodies at different combinations, and testing out positive control and no antibody/single primary antibody incubations. For example, as a positive control (detecting β-catenin) in a small cohort of samples and during PLA optimization, 1:500 active β-catenin (Cell Signaling Technology, 8814, RRID:AB_11127203) was paired with varying concentrations of β-catenin (BD Biosciences, 610154, RRID:AB_397554) or β-catenin (Invitrogen, MA1-2001, RRID:AB_326078).

Quantification of PLA signal: TMA - PLA signal was quantified on 3 20x images per replicate using a homemade macro in Fiji (25). Nuclei were quantified using the greater of the two values computed using Method 1 or 2. Method 1 - Images were deconvoluted using H&E vectors. Pink signal was thresholded at (0, 230), converted to mask, watershedded, and Analyze Particles function was used to count nuclei (minimum size 350). Method 2 - Images were deconvoluted using H&E 2 vectors. Pink signal was thresholded at (0, 230), converted to mask, watershedded, and Analyze Particles function was used to count nuclei (minimum

size 350). PLA dots were quantified as described in Method 2 with the following modifications: Blue signal was thresholded at (0, 151), and particles with size 5-100 were counted with Analyze Particles. PLA/nuclear signal was computed per image and averaged to yield normalized PLA signal for each sample. Allografts - PLA signal from allografts was quantified as described except that it was quantified on 10 40x images per mouse.

Brightfield IHC on human tissues. Brightfield IHC on human tissues was performed as described for brightfield IHC on mouse tissues with the following modifications: Blocking was performed using custom blocking buffer with subsequent M.O.M. diluent incubation step as described above for murine PLA. Primary antibodies were diluted in M.O.M. diluent (if originating in mouse) or using diluent prepared per manufacturer instructions in VECTASTAIN Elite ABC-HRP Kit, Peroxidase (Rabbit IgG) (Vector Labs, PK-6101). The following primary antibodies were used: 1:1500 SF1 (custom in-house antibody, RRID AB_2716716); 1:500 β-catenin (BD Biosciences, 610154, RRID:AB_397554); 1:50 EZH2 (Cell Signaling Technology, 5246S, RRID:AB_10694683). The M.O.M. (Mouse on Mouse) Immunodetection Kit – Basic (Vector Laboratories, BMK-2022) was used to prepare secondary antibodies for samples incubated with a primary antibody originating in mouse.

Generation and analysis of high-throughput data

Immunoprecipitation/mass spectrometry (IP-MS). NCI-H295R cells were cultured as described and plated in 10 cm dishes. To minimize biological variability, 3 ~80% confluent plates of 3 independent passages of exponentially growing cells (total 9 plates) were harvested and pooled for nuclear co-IP using the Nuclear Complex Co-IP Kit (Active Motif 54001) and Protein G Agarose Columns (Active Motif 53039). Nuclear co-IP was performed as described using aforementioned antibodies against EZH2, active β-catenin, SF1, DNMT1, or negative control IgG with the following modifications: 500 µg of pooled nuclear lysate was used for each co-IP (antibodies scaled accordingly), and co-IPs were not eluted. Instead, after final wash in IP wash buffer without BSA, samples were centrifuged at 1200xg at 4°C for 3 minutes. For a final rinse to remove residual wash buffer, 500 µL of PBS was added to each IP, samples were centrifuged at 1200xg at 4°C for 30 seconds, and Protein G columns were stored in new 1.5 mL microcentrifuge tubes and frozen at -80°C. Samples were delivered on dry ice to MS Bioworks, Ann Arbor, MI for mass spectrometry analysis using the IP-works platform.

Samples were prepared and analyzed by MS Bioworks as follows. The resin was suspended in 60 µL of 1.5X loading buffer and columns were heated to 90°C for 2 min. The column bottom plugs were removed and the boiled eluate was recovered by centrifugation at 3,000 x g for 1 min. Half of each submitted sample was processed by SDS-PAGE using a NuPAGE 10% Bis-Tris gel (Invitrogen, NP0301) with the MES buffer system (Invitrogen, NP0002). The gel was run 2 cm. The gel lane was excised into 10 equal sized segments and in-gel

digestion was performed on each using a robot (ProGest, DigiLab) with the following protocol: Washed with 25mM ammonium bicarbonate followed by acetonitrile. Reduced with 10mM dithiothreitol at 60°C followed by alkylation with 50mM iodoacetamide at RT. Digested with sequencing grade trypsin (Promega) at 37°C for 4 hours. Quenched with formic acid and the supernatant was analyzed directly without further processing.

Half of each digest was then analyzed by nano LC-MS/MS with a Waters NanoAcquity HPLC system interfaced to a ThermoFisher Q Exactive. Peptides were loaded on a trapping column and eluted over a 75 µm analytical column at 350 nL/min; both columns were packed with Luna C18 resin (Phenomenex). The mass spectrometer was operated in data-dependent mode, with the Orbitrap operating at 70,000 FWHM and 17,500 FWHM for MS and MS/MS respectively. The fifteen most abundant ions were selected for MS/MS. 5 hours of instrument time was used per sample.

Data were searched using a local copy of Mascot (Matrix Science) with the following parameters: Enzyme – Trypsin/P, Database – SwissProt Human (concatenated forward and reverse plus common contaminants), Fixed modification – Carbamidomethyl (C), Variable modifications – Oxidation (M), Acetyl (N-term), Pyro-Glu (N-term Q), Deamidation (N/Q), Mass values – Monoisotopic, Peptide Mass Tolerance – 10 ppm, Fragment Mass Tolerance – 0.02 Da, Max Missed Cleavages – 2. Mascot DAT files were parsed into Scaffold (Proteome Software) for validation, filtering and to create a non-redundant list per sample. Data were filtered using at 1% protein and peptide FDR and requiring at least two unique peptides per protein. Known contaminants and reverse hits were excluded from downstream analysis.

In this study, a protein was considered an interactor if it met the following criteria: $\geq$ 5 spectral counts in target co-IP and either not detected in IgG co-IP or at least 2-fold enrichment over IgG in target co-IP based on dividing spectral count values. Prior to submission of co-IPs for IP-MS, co-IP efficacy was verified by Coomassie staining and evaluation of *bona fide* protein interactions reported in the literature by western blot (e.g. EZH2/SUZ12, DNMT1/PCNA). The 2-fold cutoff for enrichment was determined based on the minimum threshold required to capture *bona fide* protein interactors (supported by the literature).

RNA-seq. NCI-H295R were plated in 6 well plates and treated for 96 hours as described with EZH2i at the IC-50 dose (62 µM EPZ-6438), CBPi at the IC-50 dose (26 µM PRI-724), or the vehicle (equivalent volume of DMSO, these are "baseline") in 3 biological replicates. Alternatively, NCI-H295R were plated in 6 well plates and treated with equivalent volume of vehicle (DMSO) for 48 hours and then treated with 10 µM forskolin for 48 hours as described in 3 biological replicates. mRNA and genomic DNA were extracted at endpoint for RNA-seq and 850k array profiling, respectively. RNA-seq was performed by the University of Michigan Advanced Genomics Core. Libraries were prepared from total mRNA extracted from NCI-H295R according to standard Illumina protocols using the NEBNext PolyA Ultra II RNA Library Prep Kit for Illumina. 50 bp paired-

end reads were generated in the Illumina NovaSeq-6000 platform (S1 100 cycle) at an output to ensure ~50 million reads/sample. Reads were aligned to the hg38 assembly of the human genome using STAR (RRID:SCR_004463) (31). Gene expression was quantified by featureCounts (RRID:SCR_012919) (32). Quality control metrics were generated by RNA-SeQC (RRID:SCR_005120) (33). Count data was normalized using TMM normalization from edgeR (RRID:SCR_012802) (34,35); logCPM values were generated using the voomWithQualityWeights function from limma (RRID:SCR_010943) (36). FPKM values were calculated using rpkm function from edgeR (34,35). Genes were ranked by FPKM to determine percentile of expression. GSVA (17) was used to calculate zF differentiation, cell cycle, and Wnt scores per class with genes as described in methods section detailing analysis of ACC-TCGA data. BAM files for Y1 RNA-seq were generated according to the same pipeline from fastq files downloaded from DDBJ/EMBL/GenBank DRA000853 aligned to mm10.

ATAC-seq. NCI-H295R were plated in 6 well plates and treated for 96 hours as described with EZH2i at the IC-50 dose (62 μM EPZ-6438), CBPi at the IC-50 dose (26 μM PRI-724), or the vehicle (equivalent volume of DMSO, these are "baseline") in 2 biological replicates. Alternatively, NCI-H295R were plated in 6 well plates and treated with equivalent volume of vehicle (DMSO) for 48 hours and then treated with 10 μM forskolin for 48 hours as described in 2 biological replicates. At endpoint, cells were harvested for ATAC-seq. ATAC-seq was performed as previously described (37) with modifications. Specifically, 50,000 cells were resuspended in 500 μL resuspension buffer (10 mM Tris-HCl pH 7.4, 10 mM NaCl, and 3 mM $MgCl_2$ in water). Cells were centrifuged at 50xg for 10 min in a pre-chilled (4°C) fixed-angle centrifuge. Lysis and transposition were performed simultaneously by resuspending cells in 25 μL tagmentation mix (12.5 μL 2xTD buffer [Illumina, 15027866], 1.25 μL Tn5 enzyme [Illumina, 15027865], 9.25 μL PBS, 0.5 μL 1% digitonin, 0.5 μL Tween-20, 0.5 μL NP40, and 0.5 μL 100x protease inhibitors), and incubating at 37°C for 30 min in a thermomixer with shaking at 1,000 rpm. Tn5 transposase-tagged DNA was amplified by PCR and purified using AMPure XP magnetic beads. ATAC-seq reads were sequenced 2x150 bp using a NovaSeq 6000. Sequencing of ATAC-seq libraries was performed by the University of Michigan Advanced Genomics Core.

We used bowtie2 (RRID:SCR_016368) (38) to align the reads to the hg38 version of the human genome. Reads overlapping with blacklisted regions (defined by ENCODE (1,2)), and reads with a mapping score < 20 were filtered. For ATAC-seq peak calling, we used genrich (39). For differential peak calling we used diffbind (RRID:SCR_012918) (40,41). For motif enrichment analysis we used HOMER (RRID:SCR_010881) (42). Integration of RNA-seq and ATAC-seq data was performed using diffTF (43). BigWig files were generated from merged replicates using deepTools (RRID:SCR_016366) (44) with RPGC normalization, and visualized using the JBR browser (45) or BigwigTrack from Signac (RRID:SCR_021158) (46).

ChIP-seq. NCI-H295R were plated in standard culture medium in 10 cm dishes at a density of 2.4 million cells per plate. To best account for biological variability, this experiment was performed using 24 plates of cells

total, where 16 plates were reserved for EZH2i administration at the IC-50 dose (62 μM EPZ-6438) and 8 plates were reserved for vehicle administration (equivalent volume of DMSO, these are considered "baseline" NCI-H295R). 24 hours after plating and daily thereafter, media was changed for media containing IC-50 EZH2i or vehicle. After approximately 96 hours of drug administration (120 hours post-plating), cells were harvested for ChIP-seq with *Drosophila melanogaster* histone spike-in for all epitopes according to Active Motif's Epigenetic Services ChIP Cell Fixation protocol. Briefly, media was supplemented with 1/10 media volume of freshly prepared Formaldehyde Solution (11% formaldehyde, 0.1 M NaCl, 0.5 M EDTA pH 8.0, 1 M HEPES pH 7.9 in nuclease-free water), and plate was agitated for 15 minutes at room temperature. Fixation was stopped with addition of 1/20 volume of Glycine Solution (2.5 M Glycine, MW 75 in nuclease-free water) and incubating at room temperature for 5 minutes. Cells were then scraped, collected into a conical tube, and pelleted at 800xg at 4°C for 10 minutes. Supernatant was aspirated and each tube of cells was re-suspended in 10 mL chilled PBS-Igepal (0.5% Igepal CA-630 in PBS). Cell were pelleted again, supernatant aspirated, and cells resuspended in 10 mL chilled PBS-Igepal supplemented with 100 μL of 100 mM PMSF in ethanol. Cells were pelleted again, supernatant aspirated, snap frozen on dry ice, stored at -80°C, and shipped on dry ice to Active Motif Services (Carlsbad, CA) for chromatin preparation and ChIP-seq.

In brief, chromatin was isolated by the addition of lysis buffer, followed by disruption with a Dounce homogenizer. Lysates were sonicated and DNA sheared to an average length of 300-500 bp. Genomic DNA (Input) was prepared by treating aliquots of chromatin (pooled from all submitted samples) with RNase, proteinase K and heat for de-crosslinking, followed by ethanol precipitation. Pellets were resuspended and the resulting DNA was quantified on a NanoDrop spectrophotometer. Extrapolation to the original chromatin volume allowed quantitation of the total chromatin yield.

An aliquot of chromatin (30 μg) was precleared with protein A agarose beads (Invitrogen). Genomic DNA regions of interest were immunoprecipitated using the following antibodies: EZH2 (Active Motif, 39901; concentration 8 μL Ab/30 μg chromatin), H3K27me3 (ActiveMotif, 39155, RRID:AB_2561020; concentration 4 μg Ab/30 μg chromatin), H3K27ac (ActiveMotif, 39133, RRID:AB_2561016; concentration 4 μg Ab/30 μg chromatin), SF1 (EMD Millipore, 07-618, RRID:AB_310756; concentration 5 μg Ab/30 μg chromatin) and β-catenin (Invitrogen, 71-2700, RRID:AB_2533982; concentration 4 μg Ab/30 μg chromatin)**.** Complexes were washed, eluted from the beads with SDS buffer, and subjected to RNase and proteinase K treatment. Crosslinks were reversed by incubation overnight at 65°C, and ChIP DNA was purified by phenol-chloroform extraction and ethanol precipitation. Quantitative PCR (qPCR) reactions to verify ChIP efficacy were carried out in triplicate on specific positive control genomic regions using SYBR Green Supermix (Bio-Rad).

Illumina sequencing libraries were prepared from the ChIP and Input DNAs by the standard consecutive enzymatic steps of end-polishing, dA-addition, and adaptor ligation. Steps were performed on an automated

system (Apollo 342, Wafergen Biosystems/Takara). After a final PCR amplification step, the resulting DNA libraries were quantified and sequenced on Illumina's NextSeq 500 (75 nt reads, single end).

We used bowtie2 (38) to align the reads to the hg38 version of the human genome and the dm10 version of the *Drosophila melanogaster* genome. Reads overlapping with blacklisted regions (defined by ENCODE), and reads with a mapping score < 20 were filtered. BAM files were down-sampled to account for *Drosophila* spike-in control, enabling quantitative comparison of epitopes accounting for net chromatin recruitment across treatment conditions. To perform ChIP-seq peak calling, we used SPAN and the JBR browser (45). These tools allow for empirical parameter adjustment after visual inspection of the peaks to obtain the best possible signal-to-noise ratio (FRIP). We used the annotatePeak function from the R/Bioconductor package ChIPseeker (RRID:SCR_021322) (47) to annotate the peaks according to distance to TSS and overlapping features. For motif enrichment analysis we used HOMER (42). We used bedtools (RRID:SCR_006646) (48) for identifying intersections of interest across different epitopes. BigWig files were generating using deepTools 2.0 (44) with RPGC normalization, and visualized using the JBR browser (45) or BigwigTrack from Signac (46). For visualization and quantification of the intensity of the signal across peaks of interest we used deepTools 2.0 (44). We identified super-enhancers using ROSE (RRID:SCR_017390) (49,50).

Methylation arrays. Extracted gDNA from patient samples (microdissected as in (51)) was subject to 850k array profiling performed by the University of Michigan Advanced Genomics Core. Extracted gDNA from EZH2i-/vehicle-treated NCI-H295R in biological triplicate was submitted to Diagenode Epigenomic Services, Denville, NJ, USA for Infinium MethylationEPIC Array Service (Diagenode, G02090000). DNA was deaminated using EZ-96 DNA Methylation Kit (Zymo Research) following Illumina recommendations. Bisulfite conversion was controlled by qPCR as follows: one assay targeting a methylated region of *DNAJC15* and two assays targeting *GNAS* (one assay for the unmethylated allele and one assay for the methylated allele) were used for quality control. Deaminated DNA derived from blood were amplified in parallel, and a sample passed quality control when the measured C_t for the two *GNAS* loci or *DNAJC15* is within 5 C_t of the positive control. MethylAid (RRID:SCR_002659) (52) was used on 850k array data to assess quality control, and minfi (RRID:SCR_012830) (53) was used to perform functional normalization, and generate table of beta values. Table was filtered to include CpG probes with differential methylation between fetal and adult adrenal tissues, and further filtered for probe sets of interest. PRC2 target probes were probes that fall in CpG islands annotated with genes included in the BENPORATH_PRC2_TARGETS set deposited in MSigDB (RRID:SCR_016863) (5,54,55). We used the annotatePeak function from the R/Bioconductor package ChIPseeker (47) to annotate probes according to distance to TSS and overlapping features. Copy number inference was performed using conumee (56). Statistical analysis was performed using limma (36) to assess probe-specific differential methylation.

Analysis of ACC-TCGA. Differential gene expression analysis and retrieval of expression data from ACC-TCGA data was performed as described in (4). Genes comprising zF differentiation score were identified using BioGPS (RRID:SCR_006433) and expert curation. Briefly, we selected transcripts that were highly differentially expressed in adrenal cortex compared to other organs as in (3). This list was further curated to include genes that participate in steroid production, and augmented to include genes known to participate in steroidogenesis and adrenal differentiation (*POR*, *MC2R*, and *NR5A1*). The final list of genes comprising the zF differentiation score were: *AGTR1*, *MC2R*, *LDLR*, *SOAT1*, *DHCR24*, *STAR*, *CYP11A1*, *CYP17A1*, *HSD3B2*, *CYP21A2*, *CYP11B1*, *POR*, *SULT2A1*, *CYB5B*, *ALAS1*, *FDX1*, *FDXR*, *GSTA4*, *NR5A1*, *GATA6*, *SLC47A1*, *KCNK3*, *NOV*, *INHA*, *TNXB*). Given the importance of tissue of origin in defining program activation, we used independent component analysis (ICA) (57) across ACC-TCGA samples to identify modules of co-regulated cell cycle and Wnt/β-catenin-regulated genes. The final list of genes comprising the cell cycle score were: *ISL1*, *MYBL2*, *FOXA2*, *HOXC11*, *RRM2*, *BIRC5*, *TNNT1*, *CKAP2L*, *PLAC1*, *CDC20*, *TROAP*, *CDC45*, *OTX1*, *KIF18B*, *SPRR2D*, *POU4F1*, *HOXD13*, *DHRS2*, *KIF2C*, *EXO1*, *SPC24*, *AURKB*, *CLSPN*, *LAMA1*, *KIF4A*. The final list of genes comprising the Wnt score were: *VSNL1*, *ISM1*, *PCP4*, *CALN1*, *RHCG*, *LGR5*, *MUCL1*, *SHOC1*, *COL11A1*, *COL26A1*, *CTNNA2*, *MME*, *SORCS1*, *CHL1*, *CCN3*, *SOWAHB*, *PLPPR1*, *KCNJ5*, *TAFA4*, *SPRR1A*, *CDH2*, *WNT4*, *NKD1*, *KCNC2*, *ATP2B3*.

We used GSVA (RRID:SCR_021058) (17) to calculate zF differentiation, cell cycle, and Wnt scores in ACC-TCGA samples. Final zF differentiation, cell cycle, and Wnt scores were validated on the basis of significantly higher expression in tumors with cortisol production, cell cycle pathway alterations (driver alterations in *TP53*, *RB1*, *CDKN2A*, *CCNE1*, *CDK4*), or Wnt pathway alterations (driver alterations in *CTNNB1*, *APC* or *ZNRF3*), respectively (**Supp Fig 1A-C**). Cell cycle and Wnt scores were further validated on the basis of significant correlation with *bona fide* cell cycle or Wnt pathway target genes (**Supp Fig 1D-E**). Correlograms were plotted using GGally.

Regions targeted for differential methylation in CIMP-high vs. non-CIMP-high ACC were identified using DMRcate and published in (4). Annotated significant (FDR-corrected p-value < 0.05) DMRcate regions were filtered to include only regions overlapping with promoters. Regions were ranked by descending mean difference in DNA methylation (beta fold change), and top 2084 gene identifiers (1994 NCBI Entrez Gene IDs, the maximum) were evaluated for enrichment with curated collections using GSEA (54,58). ACC-TCGA ATAC-seq BigWig files were downloaded from TCGA Genomic Data Commons (RRID:SCR_014514) (59), and signal at DMRcate regions, NCI-H295R H3K27me3 peaks, and NCI-H295R SF1/β-catenin binding sites was measured using multiBigwigSummary in deepTools (44).

Analysis of microarray data from microdissected adrenals or normal adrenals/adrenal tumors. Raw microarray data was downloaded from GEO (GSE68889) and analyzed as in (60). RMA normalization was used to obtain

expression values (61). Alternatively, processed microarray data was downloaded from GEO (GSE10927) and queried for genes of interest (*NR5A1*).

ENCODE. The following datasets were downloaded from ENCODE (RRID:SCR_006793) (1,2) for analysis in this study. Hg38 H3K27ac ChIP-seq libraries from adrenal tissue, which was analyzed to generate BigWig files and peak calls per pipeline above: ENCLB278KZX, ENCLB060VHC, ENCLB923ALY, ENCLB245VYO, ENCLB872HUE, ENCLB191XGX, ENCLB281DGJ, ENCLB670CFC, ENCLB382MNY, ENCLB198CGW, ENCLB172SDF, ENCLB735YID. Hg38 H3K27me3 ChIP-seq BigWigs +/- peak calls from embryonic stem cells and adrenal tissue: H1 - ENCFF050CUG, ENCFF671NVD; H1 MSC - ENCFF639HFP, ENCFF998IEU; H1 NSC - ENCFF202US, ENCFF495GNE; H7 - ENCFF154IMT, ENCFF662NTZ; H9 - ENCFF342DVJ, ENCFF680AKW; HUES6 - ENCFF456EQK, ENCFF725EMZ; HUES48 - ENCFF009PDQ, ENCFF612HRW; HUES64 - ENCFF015TOT, ENCFF441TOI; UCSF-4 ENCFF218TIK, ENCFF342EGR; Fetal adrenal - ENCFF250ASJ, ENCFF495YGS; Adult adrenal - ENCFF019XYA.

Analysis of single-cell RNA-seq (scRNA-seq). Gene expression matrices of human fetal, neonatal and adult adrenal scRNA-seq data (62) were downloaded from GEO (GSE134355) and filtered, normalized, batch-corrected, integrated, scaled, and UMAP clustered using Seurat (RRID:SCR_016341) with CCA integration algorithm (63). Suspected doublet cells or low-quality cells (fewer than 500 unique transcripts) were excluded. Non-adrenocortical/capsular cells (e.g. immune cells, medulla cells) were excluded by serial rounds of UMAP clustering and cluster marker identification. Gene expression was scaled so that mean expression across all cells is 0 and variance across all cells is 1, and regressed against mitochondrial content and total number of transcripts/cell. Cluster marker identification also enabled assignment of single cell clusters to known adrenocortical/capsular cell populations. Adrenocortical/capsular cells were subject to pseudotime trajectory analysis using Monocle3 (RRID:SCR_018685) (64-67), with UMAP embeddings from Seurat with origin set per figure legend.

Analysis of single-cell ATAC-seq (scATAC-seq). ScATAC-seq was processed and plotted using Signac (46) unless stated otherwise. Filtered hg38-aligned adult adrenal scATAC-seq peak matrices and fragment files were downloaded from GEO (GSM5047828) (68). Adult adrenal scATAC-seq was processed to generate peak calls, converted to hg19 with rtracklayer (69) (RRID:SCR_021325), and then normalized, LSI dimension reduced (excluding dimensions with strong correlation to sequence depth), and UMAP clustered. Filtered hg19-aligned fetal adrenal scATAC-seq peak matrices and fragment files were downloaded from Descartes Human Chromatin Accessibility During Development Atlas (70) (descartes.brotmanbaty.org) and processed as above (omitting rtracklayer step). Fetal adrenal scATAC-seq cells were downsampled to the same number of cells as in adult adrenal scATAC-seq. Fetal and adult adrenal peak sets were then merged to generate a consensus peak set, and datasets were batch-corrected, integrated, normalized, LSI dimension reduced and

UMAP clustered. Gene activity matrices were generated, and non-adrenocortical/capsular cells were excluded by serial rounds of UMAP clustering and cluster marker identification. Final clusters were compared to reference markers identified by scRNA-seq to make cluster assignments. Clusters which could not be definitively classified were grouped together and unlabeled as shown in figure.

SUPPLEMENTARY REFERENCES

1. Davis CA, Hitz BC, Sloan CA, Chan ET, Davidson JM, Gabdank I*, et al.* The Encyclopedia of DNA elements (ENCODE): data portal update. Nucleic Acids Res **2018**;46:D794-D801
2. Consortium EP. An integrated encyclopedia of DNA elements in the human genome. Nature **2012**;489:57-74
3. Zheng S, Cherniack AD, Dewal N, Moffitt RA, Danilova L, Murray BA*, et al.* Comprehensive Pan-Genomic Characterization of Adrenocortical Carcinoma. Cancer Cell **2016**;29:723-36
4. Mohan DR, Lerario AM, Else T, Mukherjee B, Almeida MQ, Vinco M*, et al.* Targeted Assessment of *G0S2* Methylation Identifies a Rapidly Recurrent, Routinely Fatal Molecular Subtype of Adrenocortical Carcinoma. Clin Cancer Res **2019**;25:3276-88
5. Ben-Porath I, Thomson MW, Carey VJ, Ge R, Bell GW, Regev A*, et al.* An embryonic stem cell-like gene expression signature in poorly differentiated aggressive human tumors. Nat Genet **2008**;40:499-507
6. Tang Z, Li C, Kang B, Gao G, Zhang Z. GEPIA: a web server for cancer and normal gene expression profiling and interactive analyses. Nucleic Acids Res **2017**;45:W98-W102
7. Baba T, Otake H, Sato T, Miyabayashi K, Shishido Y, Wang CY*, et al.* Glycolytic genes are targets of the nuclear receptor Ad4BP/SF-1. Nat Commun **2014**;5:3634
8. Walczak EM, Kuick R, Finco I, Bohin N, Hrycaj SM, Wellik DM*, et al.* Wnt signaling inhibits adrenal steroidogenesis by cell-autonomous and non-cell-autonomous mechanisms. Mol Endocrinol **2014**;28:1471-86
9. Nishimoto K, Tomlins SA, Kuick R, Cani AK, Giordano TJ, Hovelson DH*, et al.* Aldosterone-stimulating somatic gene mutations are common in normal adrenal glands. Proc Natl Acad Sci U S A **2015**;112:E4591-9
10. Trejter M, Hochol A, Tyczewska M, Ziolkowska A, Jopek K, Szyszka M*, et al.* Visinin-like peptide 1 in adrenal gland of the rat. Gene expression and its hormonal control. Peptides **2015**;63:22-9
11. Williams TA, Monticone S, Crudo V, Warth R, Veglio F, Mulatero P. Visinin-like 1 is upregulated in aldosterone-producing adenomas with KCNJ5 mutations and protects from calcium-induced apoptosis. Hypertension **2012**;59:833-9
12. Simard J, Ricketts ML, Gingras S, Soucy P, Feltus FA, Melner MH. Molecular biology of the 3beta-hydroxysteroid dehydrogenase/delta5-delta4 isomerase gene family. Endocr Rev **2005**;26:525-82
13. Stambolic V, Ruel L, Woodgett JR. Lithium inhibits glycogen synthase kinase-3 activity and mimics wingless signalling in intact cells. Curr Biol **1996**;6:1664-8
14. Seamon KB, Padgett W, Daly JW. Forskolin: unique diterpene activator of adenylate cyclase in membranes and in intact cells. Proc Natl Acad Sci U S A **1981**;78:3363-7
15. Xing Y, Edwards MA, Ahlem C, Kennedy M, Cohen A, Gomez-Sanchez CE*, et al.* The effects of ACTH on steroid metabolomic profiles in human adrenal cells. J Endocrinol **2011**;209:327-35
16. Corces MR, Granja JM, Shams S, Louie BH, Seoane JA, Zhou W*, et al.* The chromatin accessibility landscape of primary human cancers. Science **2018**;362
17. Hänzelmann S, Castelo R, Guinney J. GSVA: gene set variation analysis for microarray and RNA-seq data. BMC Bioinformatics **2013**;14:7
18. Margueron R, Li G, Sarma K, Blais A, Zavadil J, Woodcock CL*, et al.* Ezh1 and Ezh2 maintain repressive chromatin through different mechanisms. Mol Cell **2008**;32:503-18
19. Kim K, Jang I, Kim M, Choi J, Kim MS, Lee B*, et al.* 3DIV update for 2021: a comprehensive resource of 3D genome and 3D cancer genome. Nucleic Acids Res **2020**

20. Yang D, Jang I, Choi J, Kim MS, Lee AJ, Kim H*, et al.* 3DIV: A 3D-genome Interaction Viewer and database. Nucleic Acids Res **2018**;46:D52-D7

21. Borges KS, Pignatti E, Leng S, Kariyawasam D, Ruiz-Babot G, Ramalho FS*, et al.* Wnt/ β -catenin activation cooperates with loss of p53 to cause adrenocortical carcinoma in mice. Oncogene **2020**;39:5282-91

22. Giordano TJ, Kuick R, Else T, Gauger PG, Vinco M, Bauersfeld J*, et al.* Molecular classification and prognostication of adrenocortical tumors by transcriptome profiling. Clin Cancer Res **2009**;15:668-76

23. Tsherniak A, Vazquez F, Montgomery PG, Weir BA, Kryukov G, Cowley GS*, et al.* Defining a Cancer Dependency Map. Cell **2017**;170:564-76.e16

24. Drelon C, Berthon A, Mathieu M, Ragazzon B, Kuick R, Tabbal H*, et al.* EZH2 is overexpressed in adrenocortical carcinoma and is associated with disease progression. Hum Mol Genet **2016**;25:2789-800

25. Schindelin J, Arganda-Carreras I, Frise E, Kaynig V, Longair M, Pietzsch T*, et al.* Fiji: an open-source platform for biological-image analysis. Nat Methods **2012**;9:676-82

26. Pham TND, Kumar K, DeCant BT, Shang M, Munshi SZ, Matsangou M*, et al.* Induction of MNK Kinase-dependent eIF4E Phosphorylation by Inhibitors Targeting BET Proteins Limits Efficacy of BET Inhibitors. Mol Cancer Ther **2019**;18:235-44

27. Bayliss J, Mukherjee P, Lu C, Jain SU, Chung C, Martinez D*, et al.* Lowered H3K27me3 and DNA hypomethylation define poorly prognostic pediatric posterior fossa ependymomas. Sci Transl Med **2016**;8:366ra161

28. Panwalkar P, Clark J, Ramaswamy V, Hawes D, Yang F, Dunham C*, et al.* Immunohistochemical analysis of H3K27me3 demonstrates global reduction in group-A childhood posterior fossa ependymoma and is a powerful predictor of outcome. Acta Neuropathol **2017**

29. Chung C, Sweha SR, Pratt D, Tamrazi B, Panwalkar P, Banda A*, et al.* Integrated Metabolic and Epigenomic Reprograming by H3K27M Mutations in Diffuse Intrinsic Pontine Gliomas. Cancer Cell **2020**

30. Schneider CA, Rasband WS, Eliceiri KW. NIH Image to ImageJ: 25 years of image analysis. Nat Methods **2012**;9:671-5

31. Dobin A, Davis CA, Schlesinger F, Drenkow J, Zaleski C, Jha S*, et al.* STAR: ultrafast universal RNA-seq aligner. Bioinformatics **2013**;29:15-21

32. Liao Y, Smyth GK, Shi W. featureCounts: an efficient general purpose program for assigning sequence reads to genomic features. Bioinformatics **2014**;30:923-30

33. DeLuca DS, Levin JZ, Sivachenko A, Fennell T, Nazaire MD, Williams C*, et al.* RNA-SeQC: RNA-seq metrics for quality control and process optimization. Bioinformatics **2012**;28:1530-2

34. McCarthy DJ, Chen Y, Smyth GK. Differential expression analysis of multifactor RNA-Seq experiments with respect to biological variation. Nucleic Acids Res **2012**;40:4288-97

35. Robinson MD, McCarthy DJ, Smyth GK. edgeR: a Bioconductor package for differential expression analysis of digital gene expression data. Bioinformatics **2010**;26:139-40

36. Ritchie ME, Phipson B, Wu D, Hu Y, Law CW, Shi W*, et al.* limma powers differential expression analyses for RNA-sequencing and microarray studies. Nucleic Acids Res **2015**;43:e47

37. Corces MR, Trevino AE, Hamilton EG, Greenside PG, Sinnott-Armstrong NA, Vesuna S*, et al.* An improved ATAC-seq protocol reduces background and enables interrogation of frozen tissues. Nature Methods **2017**;14:959-62

38. Langmead B, Salzberg SL. Fast gapped-read alignment with Bowtie 2. Nat Methods **2012**;9:357-9

39. Gaspar JM. 2018 Genrich: detecting sites of genomic enrichment. <https://github.com/jsh58/Genrich>.

40. Ross-Innes CS, Stark R, Teschendorff AE, Holmes KA, Ali HR, Dunning MJ*, et al.* Differential oestrogen receptor binding is associated with clinical outcome in breast cancer. Nature **2012**;481:389-93

41. Stark R, Brown G. DiffBind: differential binding analysis of ChIP-Seq peak data., Bioconductor2011.

42. Heinz S, Benner C, Spann N, Bertolino E, Lin YC, Laslo P*, et al.* Simple combinations of lineage-determining transcription factors prime cis-regulatory elements required for macrophage and B cell identities. Mol Cell **2010**;38:576-89

43. Berest I, Arnold C, Reyes-Palomares A, Palla G, Rasmussen KD, Giles H*, et al.* Quantification of Differential Transcription Factor Activity and Multiomics-Based Classification into Activators and Repressors: diffTF. Cell Rep **2019**;29:3147-59.e12

44. Ramírez F, Ryan DP, Grüning B, Bhardwaj V, Kilpert F, Richter AS*, et al.* deepTools2: a next generation web server for deep-sequencing data analysis. Nucleic Acids Res **2016**;44:W160-5

45. Shpynov O, Dievskii A, Chernyatchik R, Tsurinov P, Artyomov MN. Semi-supervised peak calling with SPAN and JBR Genome Browser. Bioinformatics **2021**

46. Stuart T, Srivastava A, Madad S, Lareau CA, Satija R. Single-cell chromatin state analysis with Signac. Nat Methods **2021**;18:1333-41

47. Yu G, Wang LG, He QY. ChIPseeker: an R/Bioconductor package for ChIP peak annotation, comparison and visualization. Bioinformatics **2015**;31:2382-3

48. Quinlan AR, Hall IM. BEDTools: a flexible suite of utilities for comparing genomic features. Bioinformatics **2010**;26:841-2

49. Whyte WA, Orlando DA, Hnisz D, Abraham BJ, Lin CY, Kagey MH*, et al.* Master transcription factors and mediator establish super-enhancers at key cell identity genes. Cell **2013**;153:307-19

50. Lovén J, Hoke HA, Lin CY, Lau A, Orlando DA, Vakoc CR*, et al.* Selective inhibition of tumor oncogenes by disruption of super-enhancers. Cell **2013**;153:320-34

51. Rege J, Nakamura Y, Wang T, Merchen TD, Sasano H, Rainey WE. Transcriptome profiling reveals differentially expressed transcripts between the human adrenal zona fasciculata and zona reticularis. J Clin Endocrinol Metab **2014**;99:E518-27

52. van Iterson M, Tobi EW, Slieker RC, den Hollander W, Luijk R, Slagboom PE*, et al.* MethylAid: visual and interactive quality control of large Illumina 450k datasets. Bioinformatics **2014**;30:3435-7

53. Aryee MJ, Jaffe AE, Corrada-Bravo H, Ladd-Acosta C, Feinberg AP, Hansen KD*, et al.* Minfi: a flexible and comprehensive Bioconductor package for the analysis of Infinium DNA methylation microarrays. Bioinformatics **2014**;30:1363-9

54. Subramanian A, Tamayo P, Mootha VK, Mukherjee S, Ebert BL, Gillette MA*, et al.* Gene set enrichment analysis: a knowledge-based approach for interpreting genome-wide expression profiles. Proc Natl Acad Sci U S A **2005**;102:15545-50

55. Liberzon A, Subramanian A, Pinchback R, Thorvaldsdóttir H, Tamayo P, Mesirov JP. Molecular signatures database (MSigDB) 3.0. Bioinformatics **2011**;27:1739-40

56. Hovestadt V, Zapatka M. conumee: Enhanced copy-number variation analysis using Illumina DNA methylation arrays. R package version 1.9.02020.

57. Biton A, Bernard-Pierrot I, Lou Y, Krucker C, Chapeaublanc E, Rubio-Pérez C*, et al.* Independent component analysis uncovers the landscape of the bladder tumor transcriptome and reveals insights into luminal and basal subtypes. Cell Rep **2014**;9:1235-45

58. Mootha VK, Lindgren CM, Eriksson KF, Subramanian A, Sihag S, Lehar J*, et al.* PGC-1alpha-responsive genes involved in oxidative phosphorylation are coordinately downregulated in human diabetes. Nat Genet **2003**;34:267-73

59. NCI. 2005-2018 The Cancer Genome Atlas. National Cancer Institute <https://www.cancer.gov/tcga>.

60. Finco I, Lerario AM, Hammer GD. Sonic Hedgehog and WNT Signaling Promote Adrenal Gland Regeneration in Male Mice. Endocrinology **2018**;159:579-96

61. Irizarry RA, Hobbs B, Collin F, Beazer-Barclay YD, Antonellis KJ, Scherf U*, et al.* Exploration, normalization, and summaries of high density oligonucleotide array probe level data. Biostatistics **2003**;4:249-64

62. Han X, Zhou Z, Fei L, Sun H, Wang R, Chen Y*, et al.* Construction of a human cell landscape at single-cell level. Nature **2020**;581:303-9

63. Stuart T, Butler A, Hoffman P, Hafemeister C, Papalexi E, Mauck WM*, et al.* Comprehensive Integration of Single-Cell Data. Cell **2019**;177:1888-902.e21

64. Cao J, Spielmann M, Qiu X, Huang X, Ibrahim DM, Hill AJ*, et al.* The single-cell transcriptional landscape of mammalian organogenesis. Nature **2019**;566:496-502

65. Qiu X, Mao Q, Tang Y, Wang L, Chawla R, Pliner HA*, et al.* Reversed graph embedding resolves complex single-cell trajectories. Nat Methods **2017**;14:979-82

66. Qiu X, Hill A, Packer J, Lin D, Ma YA, Trapnell C. Single-cell mRNA quantification and differential analysis with Census. Nat Methods **2017**;14:309-15

67. Trapnell C, Cacchiarelli D, Grimsby J, Pokharel P, Li S, Morse M*, et al.* The dynamics and regulators of cell fate decisions are revealed by pseudotemporal ordering of single cells. Nat Biotechnol **2014**;32:381-6

68. Zhang K, Hocker JD, Miller M, Hou X, Chiou J, Poirion OB*, et al.* A single-cell atlas of chromatin accessibility in the human genome. Cell **2021**;184:5985-6001.e19

69. Lawrence M, Gentleman R, Carey V. rtracklayer: an R package for interfacing with genome browsers. Bioinformatics **2009**;25:1841-2

70. Domcke S, Hill AJ, Daza RM, Cao J, O'Day DR, Pliner HA*, et al.* A human cell atlas of fetal chromatin accessibility. Science **2020**;370